Chapter – 3

Microstructure of Ultrafine-Grained Low Carbon Steel

3.1 Microstructure of Equal-Channel Angular Pressed Low Carbon Steel

The microstructure of as-received low carbon steel comprises of ferrite grains of an average size of 67±7 μm with a small volume fraction of pearlite (Figure 3.1 (a)). On ECAP of the steel, ferrite grains get elongated in the extrusion direction in the initial stage of deformation (ε_{vm} = 0.6), and the grains split into deformation bands (Figure 3.1(b)).

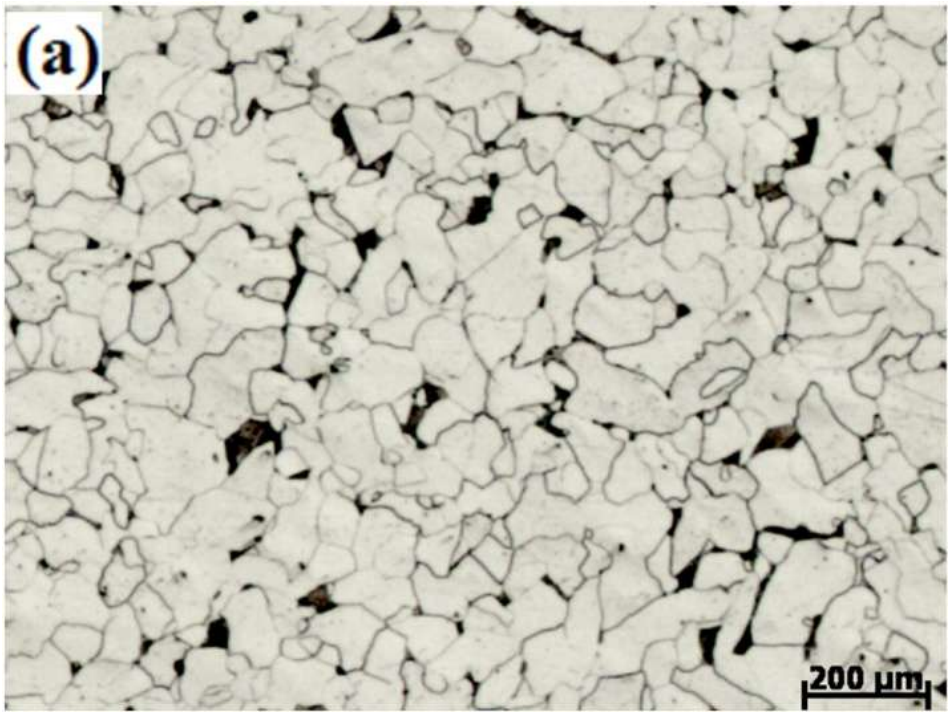

Figure 3.1: (a) Optical microstructure of the as-received low carbon steel.

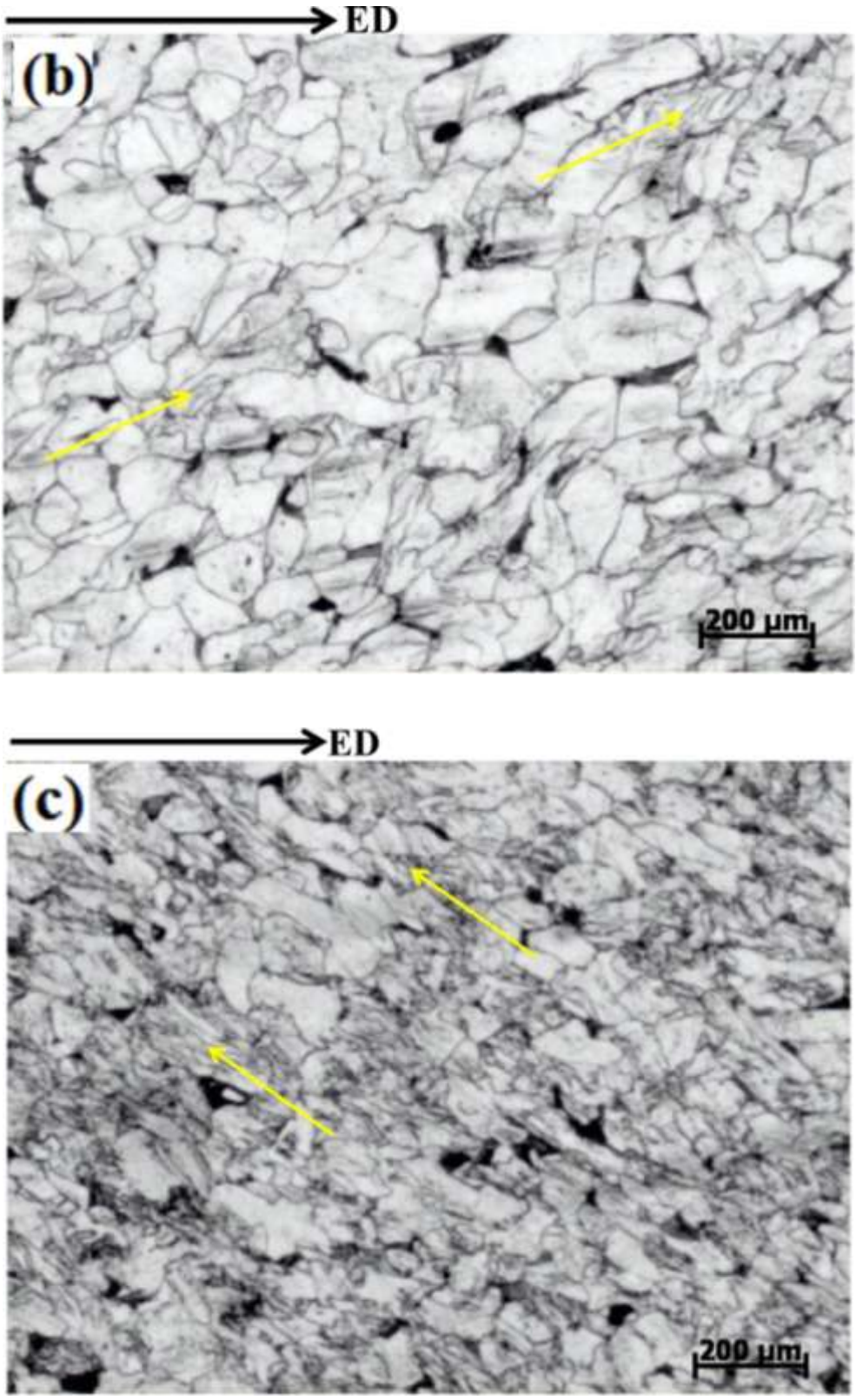

Figure 3.1: Optical microstructure of the low carbon steel in (b) ECAP-0.6, and (c) ECAP-1.2 conditions. Upside arrow is showing extrusion direction and aroow heads inside the micrograph are showing the bands.

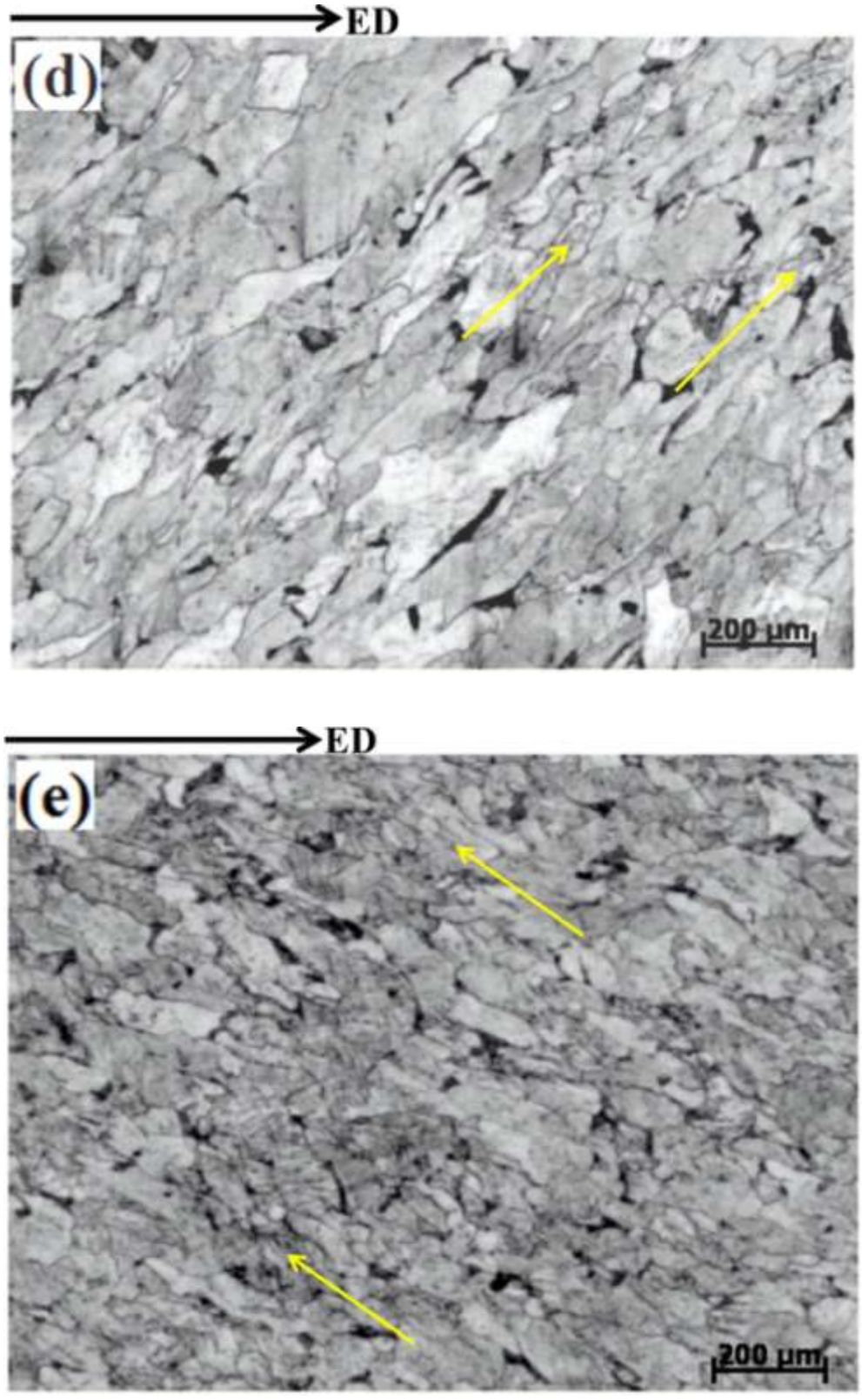

Figure 3.1: Optical microstructure of the low carbon steel in (d) ECAP-1.8, and (e) ECAP-3 conditions. Upside arrow is showing extrusion direction and aroow heads inside the micrograph are showing the bands

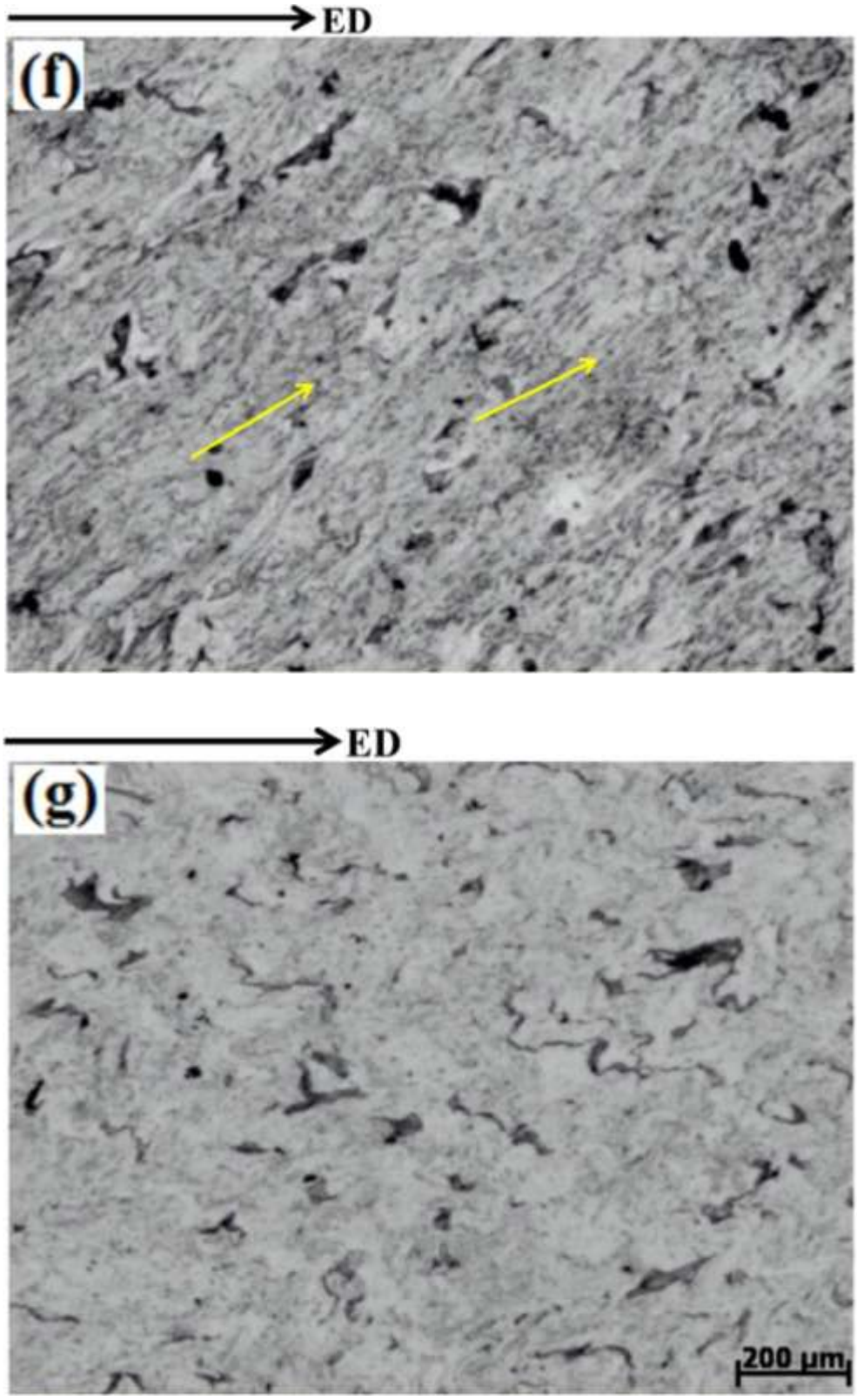

Figure 3.1: Optical microstructure of the low carbon steel in (f) ECAP-6, and (g) ECAP-9 conditions. Upside arrow is showing extrusion direction and aroow heads inside the micrograph are showing the bands

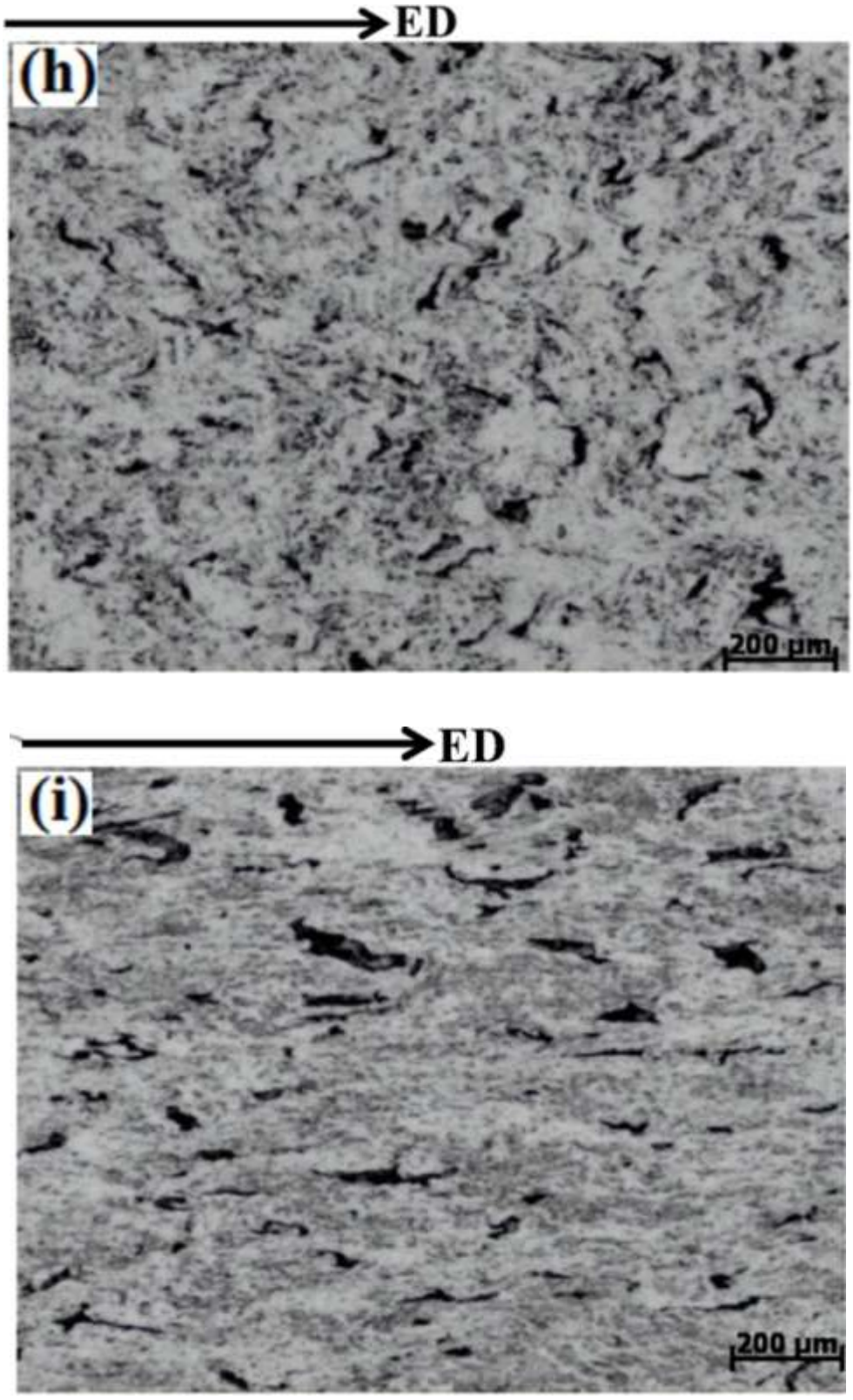

Figure 3.1: Optical microstructure of the low carbon steel in (h) ECAP-12 and (i) ECAP-16.8 conditions. Upside arrow is showing extrusion direction and aroow heads inside the micrograph are showing the bands

At ε_{vm} = 1.2, the width of the deformation bands decreases (Figure 3.1(c)). At ε_{vm} = 1.8, the thickness of elongated bands reduces but still visible in the optical micrograph (Figure 3.1(d)). At ε_{vm}=3, randomization of directions of grains takes place due to fragmentation process (Figure 3.1(e)). Beyond ε_{vm}=3 ferrite boundaries are not visible due to a large reduction in band thickness, but pearlite is scattered at the boundaries of the grains (Figures 3.1(f)-(i)).

The as-received steel displays pearlitic structure of 220 nm inter-lamellar spacing with cementite plate width of 109 μm (Figure 3.2(a)). ECAP of low carbon steel for equivalent strain 1.2, distorts pearlite into wavy form (Figure 3.2(b)). Increasing strain also reduces inter-lamellar spacing. At ε_{vm} = 6, cementite is partially dissolved in ferrite and partly broken down into tiny particles (Figure 3.2(c)). Therefore, the width of cementite plates gets reduced, and some broken cementite plates are spheroidised. The average size of cementite spheroids is 150 nm. At ε_{vm} = 9, the diameter of spherodized cementite further decreases to 140 nm due to partial dissolution and continues to do so with increase in strain (Figures 3.2(d)-(f)). Dissolution of carbides can be seen clearly (shown by arrows) at ε_{vm} = 12 in the TEM bright field image (Figure 3.2(g)), where, sharp edges of cementite become rough (Figure 3.2(g)). At ε_{vm} = 12, the diameter of spheroidized cementite reduces to 120 nm, and further decreases to 90 nm at ε_{vm} = 16.8. However lamellar pearlite colonies are not eliminated in the maximum strain level reached.

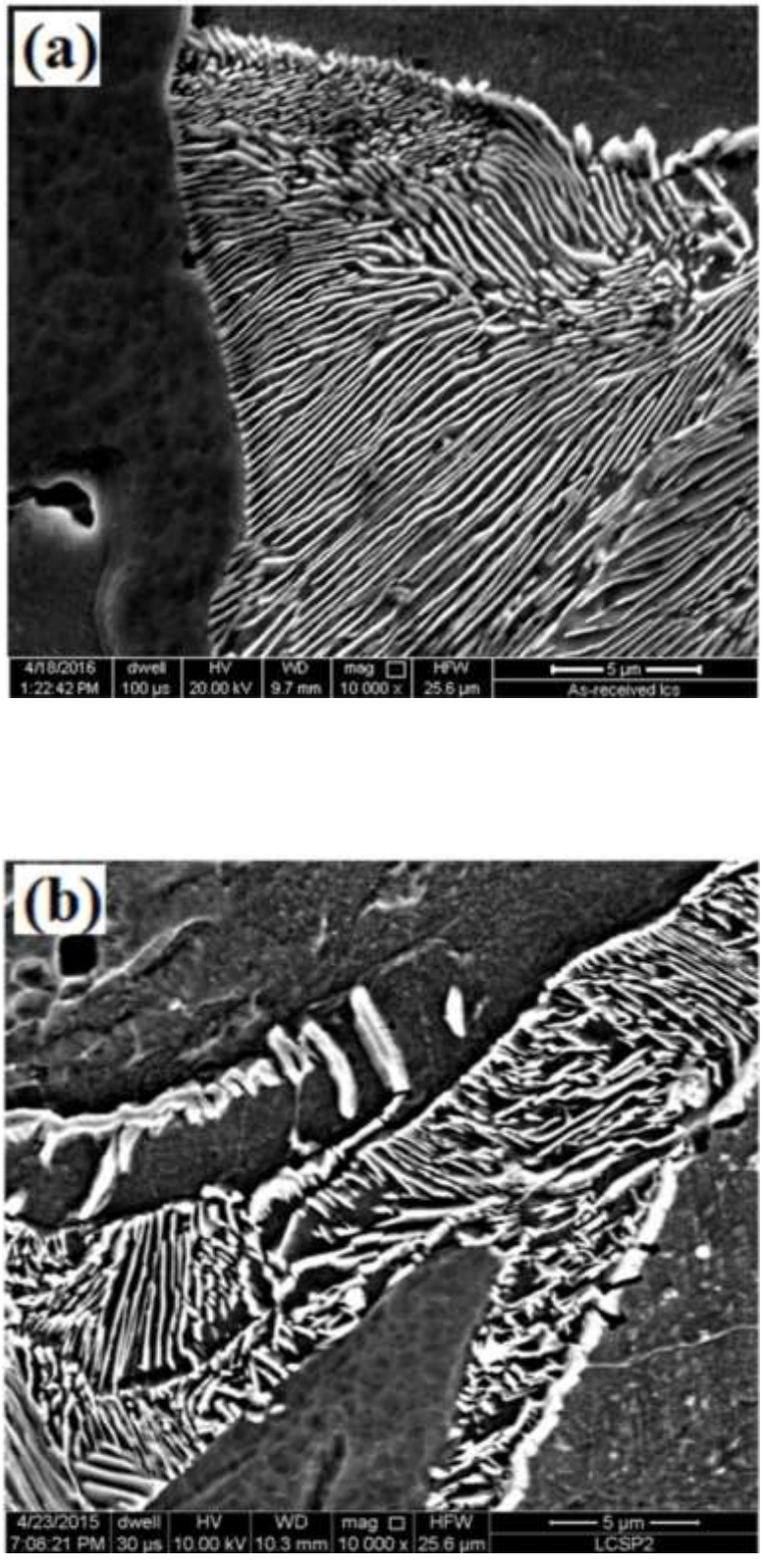

Figure 3.2: SEM micrographs (pearlitic region) of low carbon steel (a) As-received, and (b) ECAP-1.2.

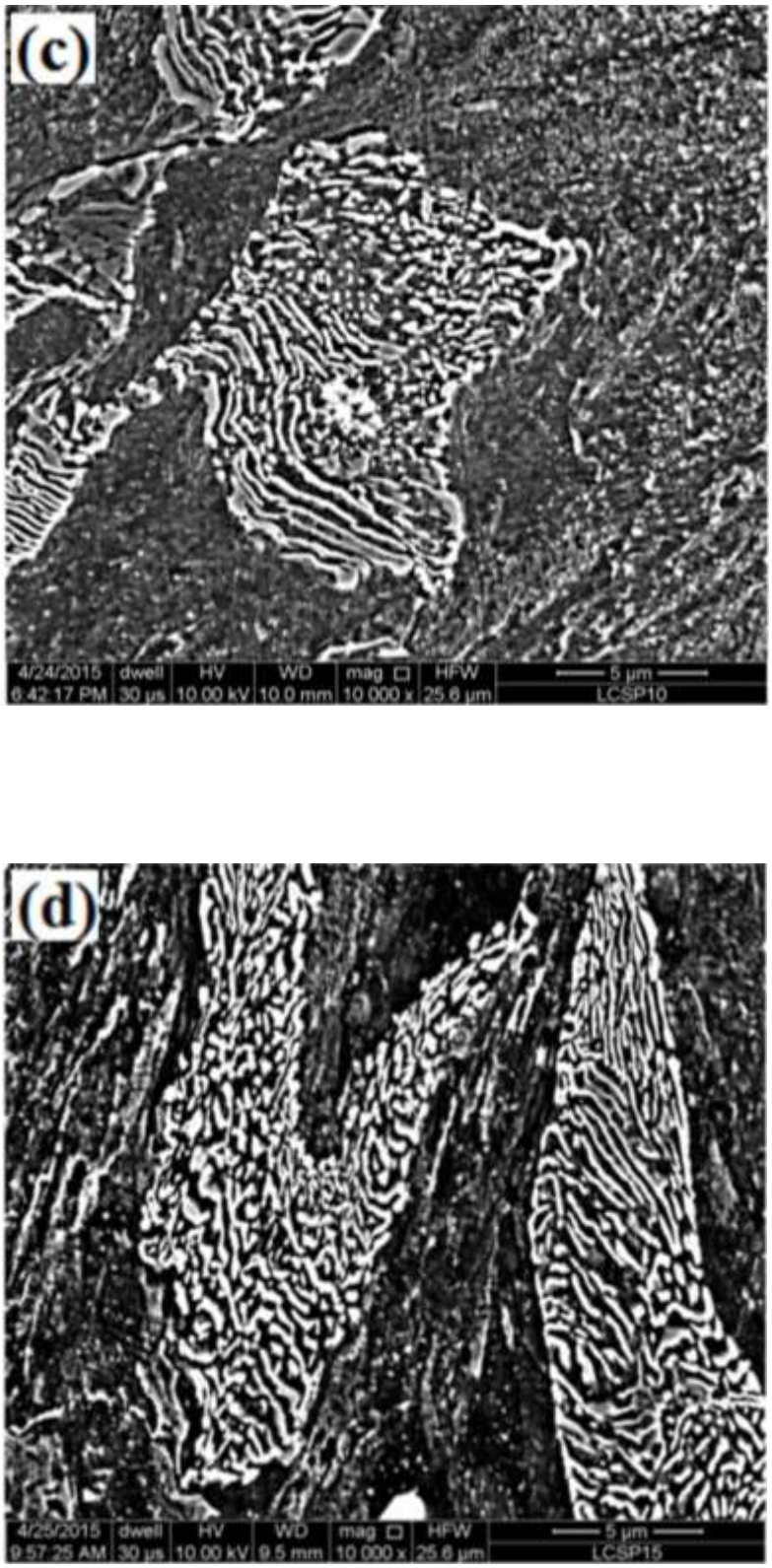

Figure 3.2: SEM micrographs (pearlitic region) of low carbon steel (c) ECAP-6, and (d) ECAP-9.

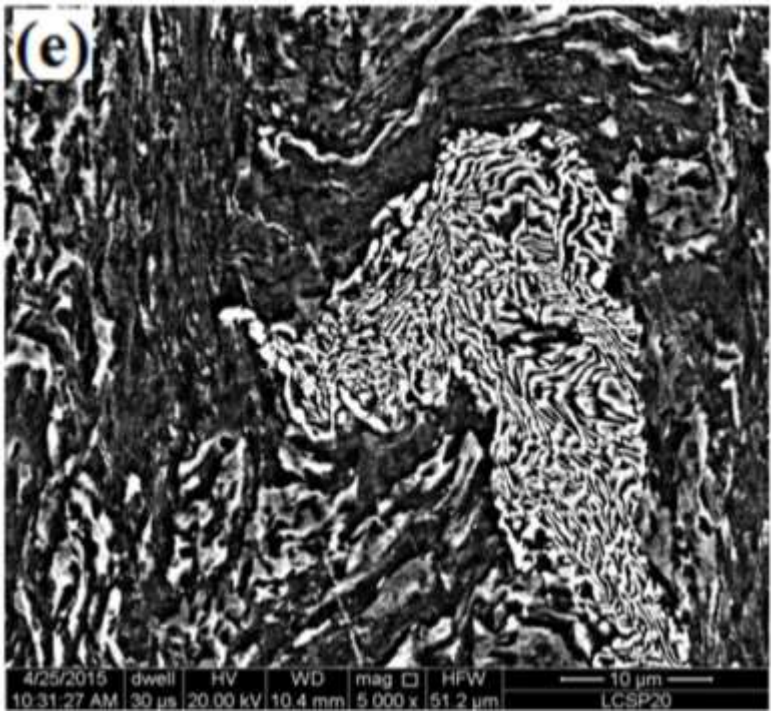

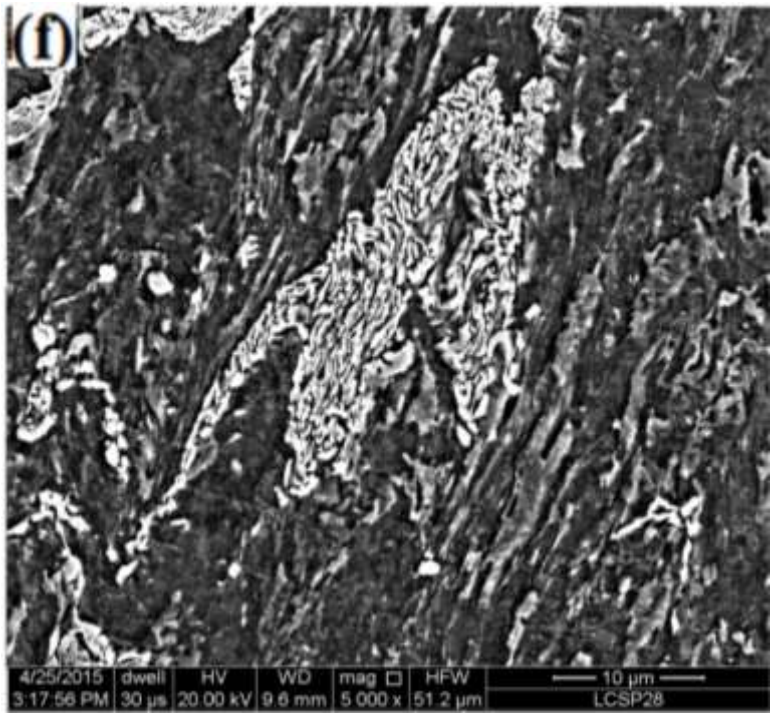

Figure 3.2: SEM micrographs (pearlitic region) of low carbon steel (e) ECAP-12, and (f) ECAP-16.8.

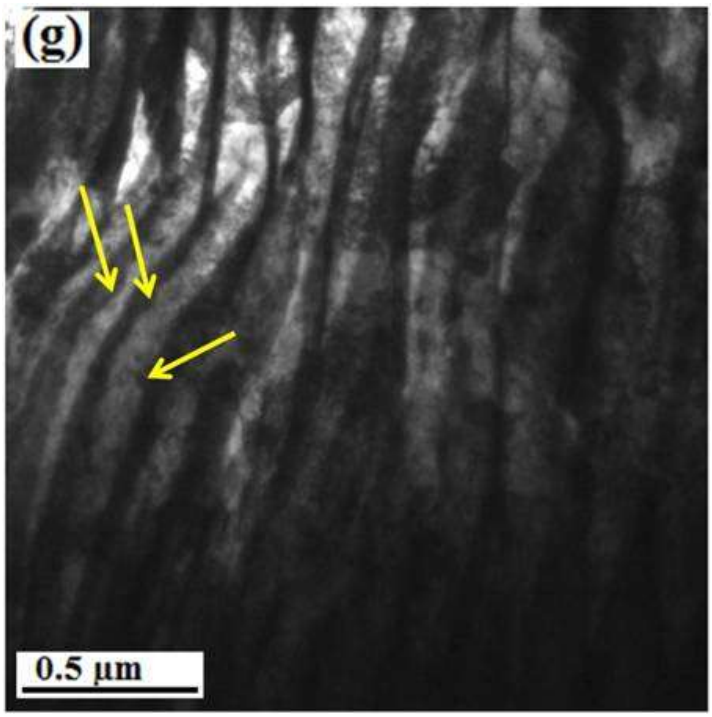

Figure 3.2: (g) TEM bright field of ECAP-12, arrows are showing dissolution of carbides form pearlite.

Figures 3.3(a-i) display the Image quality (IQ) maps of low carbon steel, where the low angle and high angle grain boundaries are traced by red lines and blue lines respectively. IQ map of as-received low carbon steel reveals the presence of low angle grain boundary fraction of 19.1% and an average misorientation angle of 35.5º (Figure 3.3(a), Table 3.1). At $\varepsilon_{vm} = 0.6$, the grains get deformed into banded structures with high defect density (Figure 3.3(b)). Some of the defects align themselves into low energy configurations, therefore, LAGB fraction increases to 74% and average misorientation angle decreases to 13.7º. At $\varepsilon_{vm} = 1.2$, the thickness of the bands gets reduced, and low angle boundaries are formed. There is an increase in defect density which is scattered in the interior of the bands (Figure 3.3(c)). Average misorientation angle further decreases to 11.62º and LAGB fraction increases to 79.9%.

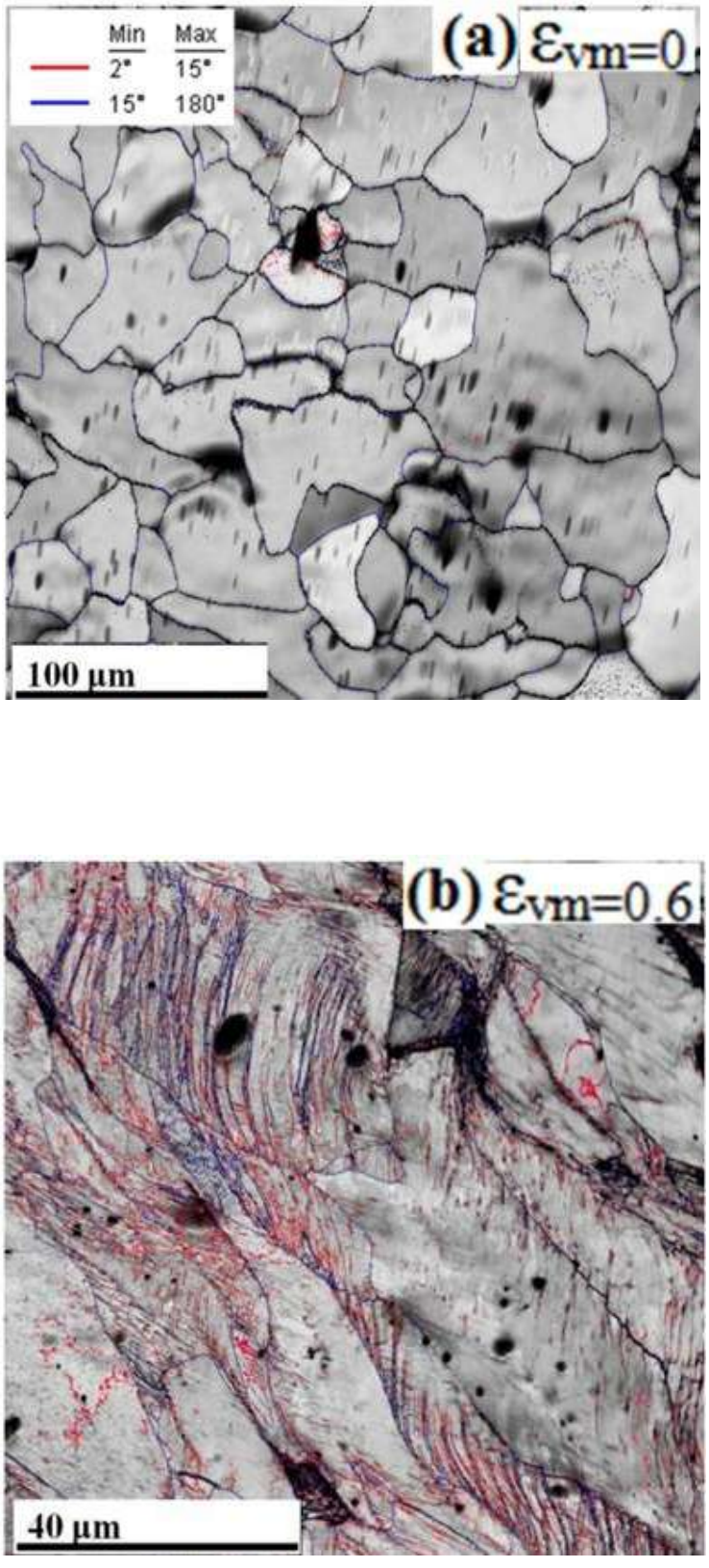

Figure 3.3: Image quality maps of low carbon steel of (a) ECAP-0, and (b) ECAP-0.6.

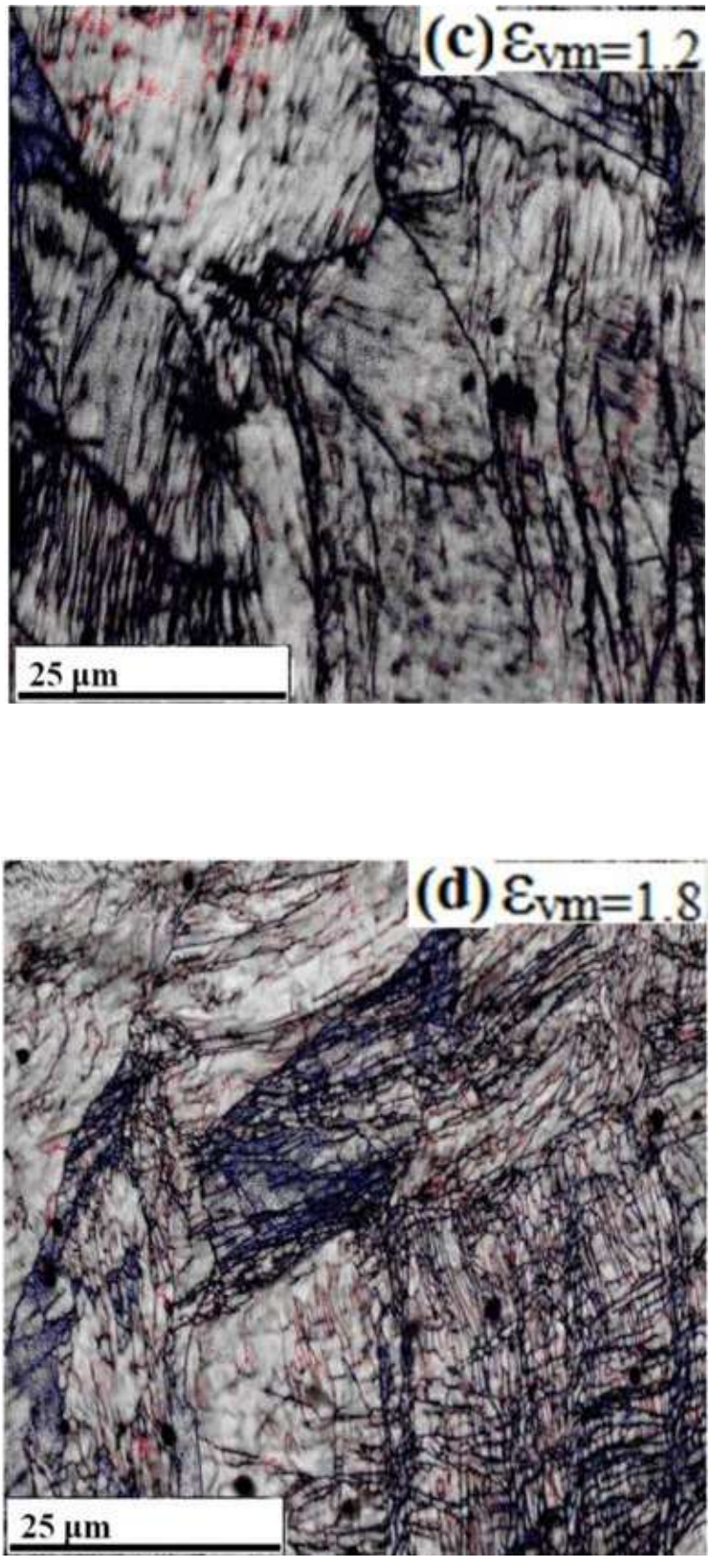

Figure 3.3: Image quality maps of low carbon steel of (c) ECAP-1.2, and (d) ECAP-1.8.

At ε_{vm} = 1.8, intersection of the bands takes place, and average misorientation angle increases to 23.3º, as a result of decrease in LAGB fraction starts decreasing (Figure 3.3(d), Table 3.1).

Table 3.1: Details of microstructural parameters of as-received and ECAPed low carbon steels.

Samples	Average grain size (μm)	LAGB Fraction (%)	Avg Misorientation Angle (º)	Crystallite size (nm)	Strain	Dislocation Density /m^2
ECAP-0	67±7	19.1	35.5	137±0.88	0.18±0.026	1.8 x10^{14}±8x10^{3}
ECAP-0.6	0.62±0.11	74	13.7	40±0.17	0.3±0.0032	10.3 x10^{14}±1.8x10^{5}
ECAP-1.2	0.42±0.1	79.9	11.62	37±0.16	0.28±0.0033	10.8 x10^{14}±1.6x10^{5}
ECAP-1.8	0.39±0.05	50.3	23.29	24±0.28	0.48±0.017	28.4 x10^{14}±8.6x10^{4}
ECAP-3	0.23±0.04	13.7	31.75	33±0.17	0.34±0.0029	14.2 x10^{14}±1.8x10^{4}
ECAP-6	0.21±0.07	63.1	17.29	33±0.15	0.36±0.0033	15.1 x10^{14}±2.1x10^{5}
ECAP-9	0.19±0.06	42.3	26.58	34±0.16	0.35±0.0028	14.7 x10^{14}±2x10^{5}
ECAP-12	0.20±0.05	27.6	34.89	31±0.17	0.40±0.0033	18.2 x10^{14}±2x10^{5}
ECAP-16.8	0.19±0.04	17.6	40.79	29±0.15	0.36±0.0034	17.1 x10^{14}±2.1x10^{5}

At ε_{vm} = 3, inhomogeniety in microstructure is observed but the band thickness is reduced with an increase in misorientation angle and transformation of cell structures into grains takes place (shown by blue lines) (Figure 3.3(e)) with the decrease in LAGB fraction to 13.7%. Average misorientation increases to 31.8º.

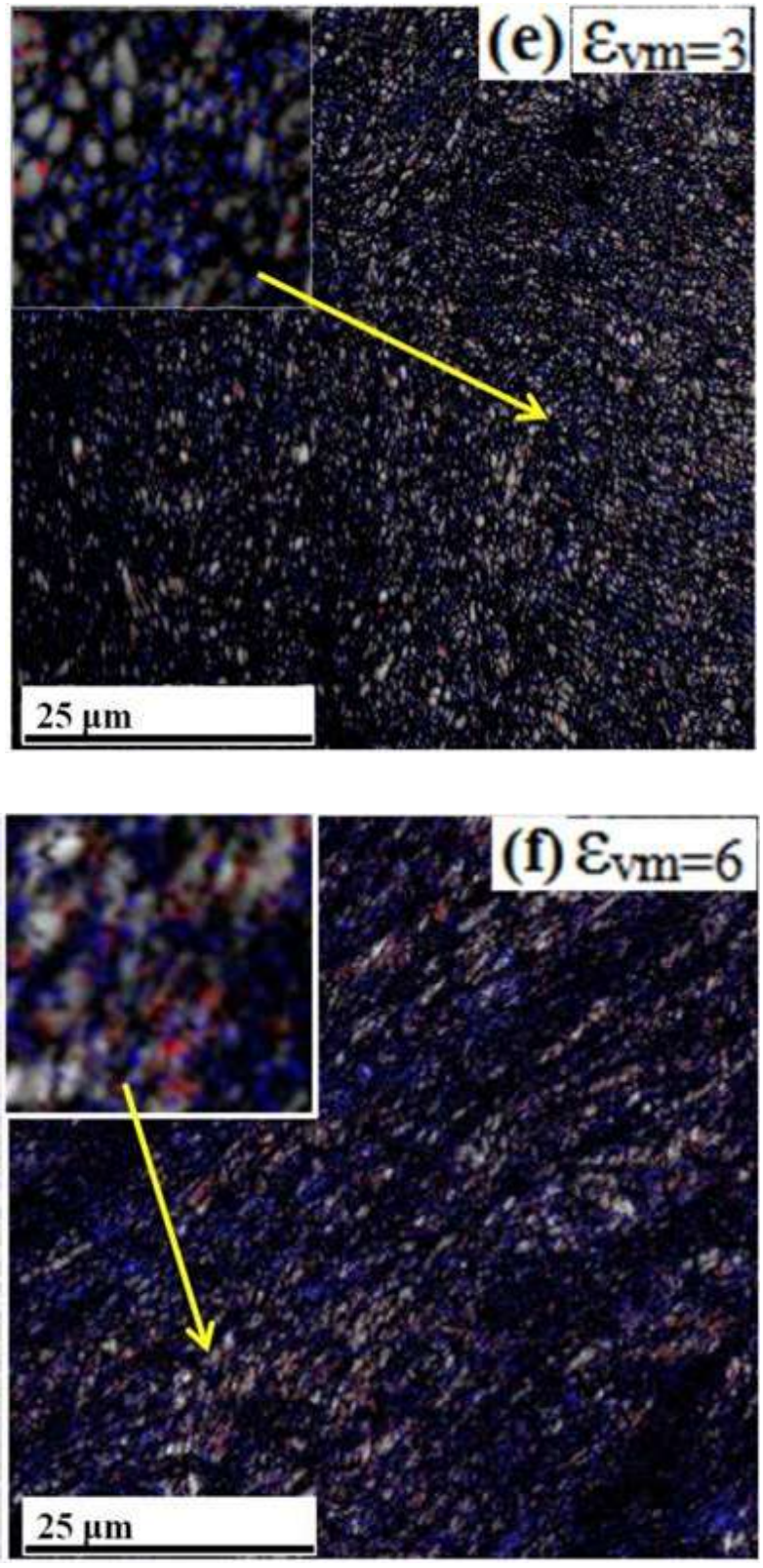

Figure 3.3: Image quality maps of low carbon steel of (e) ECAP-3, and (f) ECAP-6 samples. Magnified view of selected area shown by arrow is given in the inset of corresponding image and arrow showing the selected area.

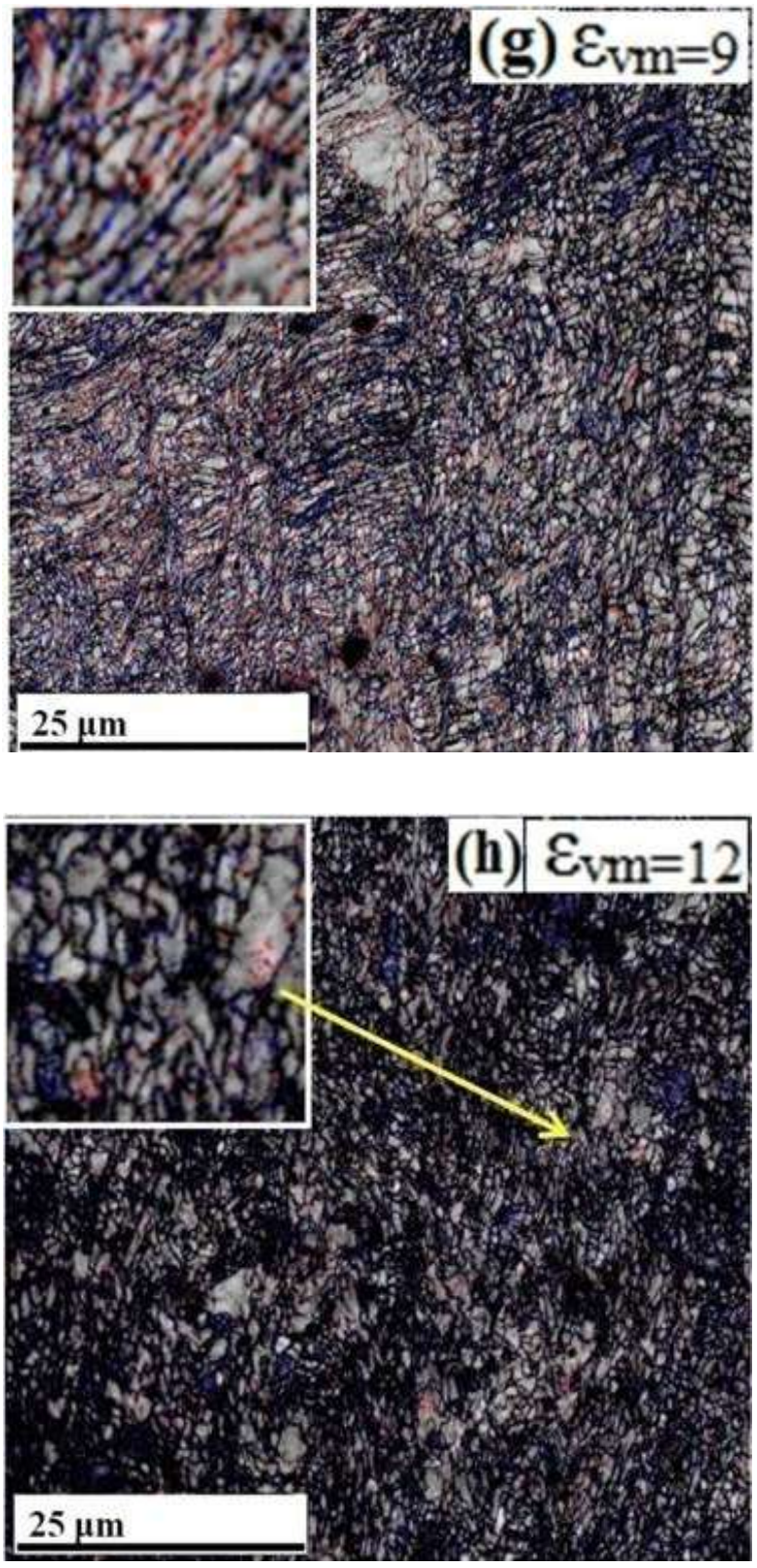

Figure 3.3: Image quality maps of low carbon steel of (g) ECAP-9, and (h) ECAP-12 samples.

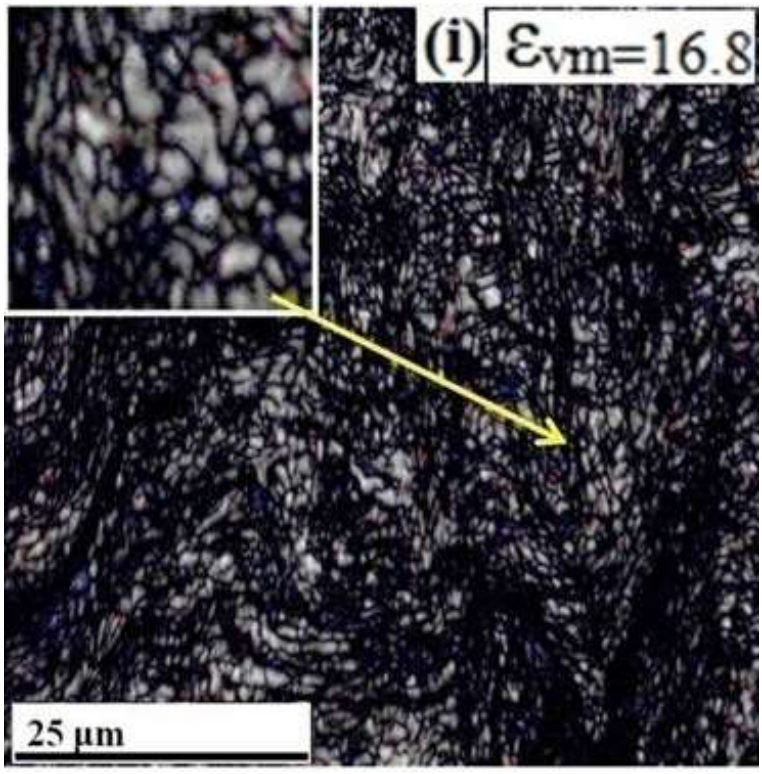

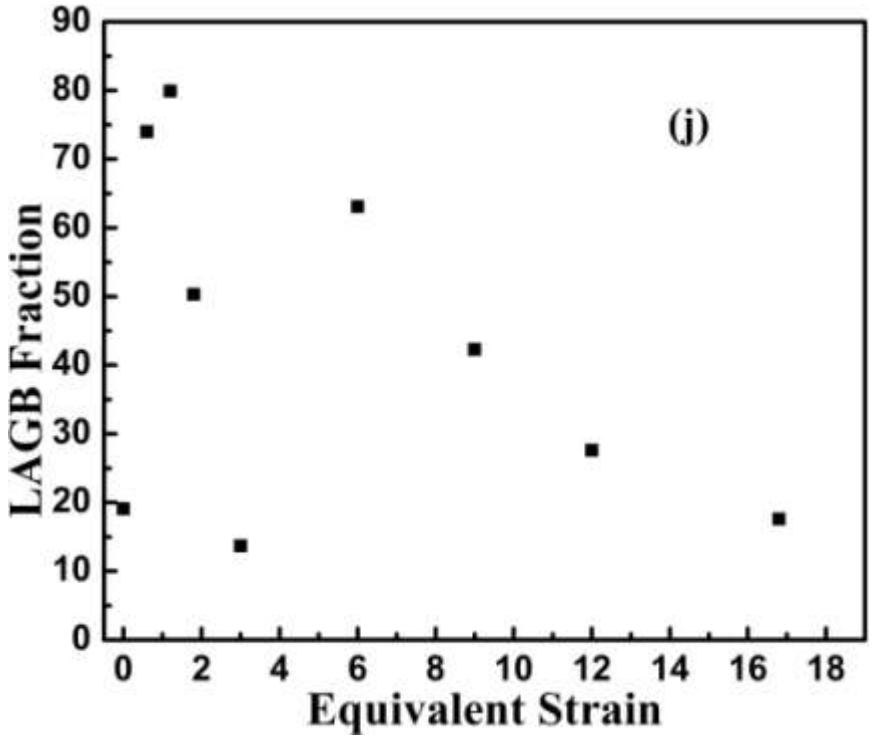

Figure 3.3: Image quality maps of low carbon steel of (i) ECAP-16.8, (j) Variation of LAGB of low carbon steel with equivalent strain.

At ε_{vm} = 6 LAGB fraction increases to 63.1%. The intersected bands developed at ε_{vm} = 1.8, get aligned towards deformation direction, and thickness of the bands also comes down at ε_{vm} = 6 . The existing high-angle boundaries, band boundaries, and cell boundaries get aligned along the deformation direction, and the structure is named as lamellar structure (Figure 3.3(f)). At ε_{vm} = 9, the spacing of lamellae decreases to one or two subgrain width and these fine very long bands are now named as ribbon grains (Figure 3.3(g)). The LAGB fraction decreases to 42.3% (Table 3.1). At ε_{vm} = 12, the ribbon grains start breaking down due to the intersection and form near-equiaxed grains (Figure 3.3(h)). The ribbon grains and newly formed equiaxed grains attain the high angle of misorientation, and as a result, the high fraction of HAGBs is increased, and thereby LAGB decreases to 27.6%. At ε_{vm} = 16.8, most of the ribbon grains and near-equiaxed grains attain a high angle of misorientation with LAGB fraction reducing to 17.6% (Figure 3.3(i)).

Figures 3.4(a-i) represent the variation in the misorientation angle with number fraction of grains sampled for the as-received and ECAPed samples subjected to different equivalent strains. Grains of the as-received low carbon steel have high average misorientation angle of 35.5° (Figure 3.4(a)). On ECAP at ε_{vm} = 0.6, the low angle boundaries are formed and the average misorientation decreases to 13.7° (Figure 3.4(b)). After ECAP for ε_{vm} = 1.2 the misorientation angle further decreases and reaches to a minimum (Figure 3.4(c)). On continuing ECAP for ε_{vm} = 1.8, the low angle boundaries begin converting to high angle boundaries (Figure 3.4(d)). The average misorientation angle shows progressively increasing trend with further increase in equivalent strain owing to the conversion of low angle boundaries to high angle boundaries. It reaches to a high value of 40.8° at ε_{vm} = 16.8 (Figure 3.4(i)).

Figure 3.4(j) show the variation of LAGB fraction of low carbon steel with equivalent strain.

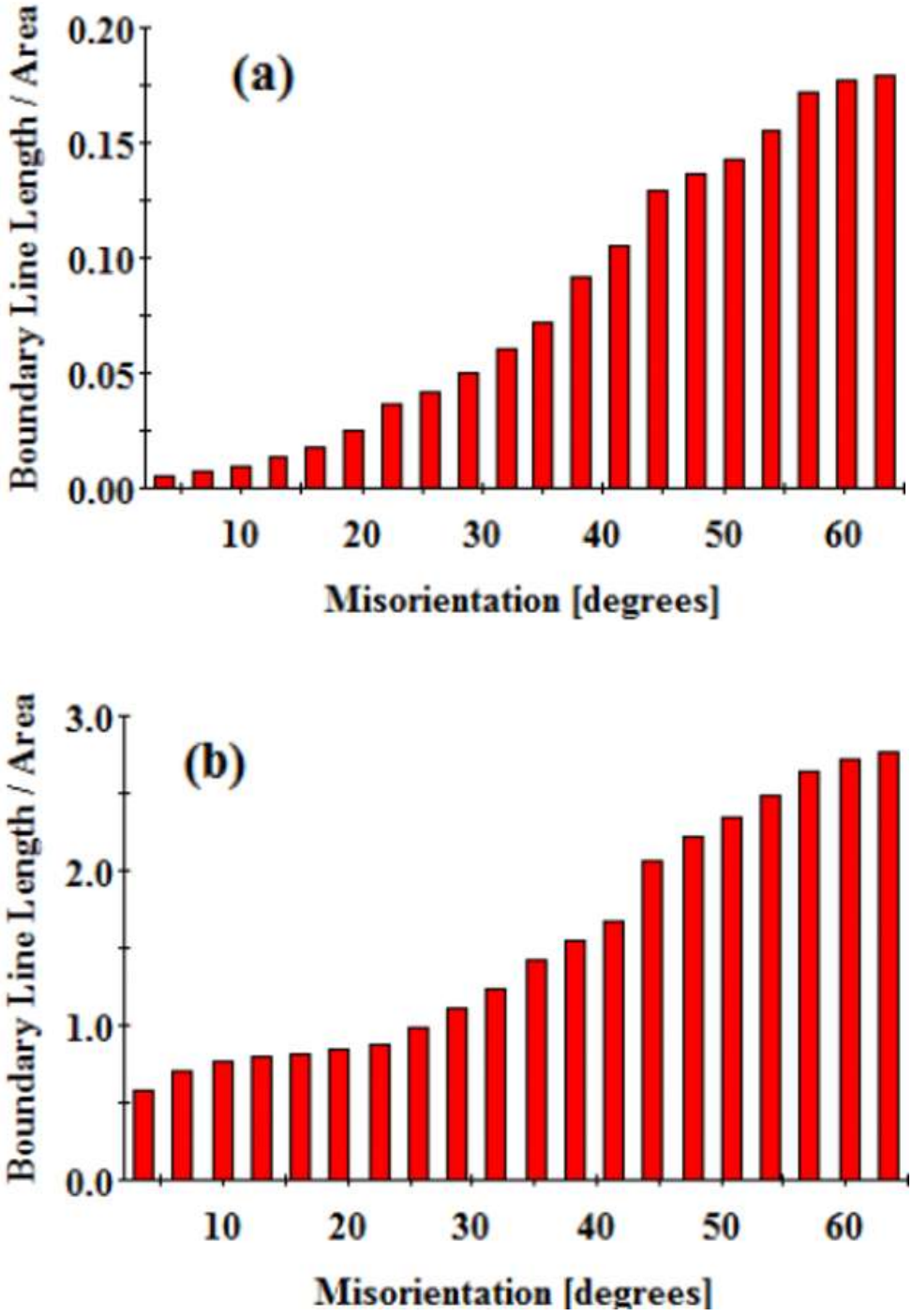

Figure 3.4: Grain boundary length/ unit area with misorientation angle distribution of low carbon steel of (a) As-received (b) ECAP-0.6 samples.

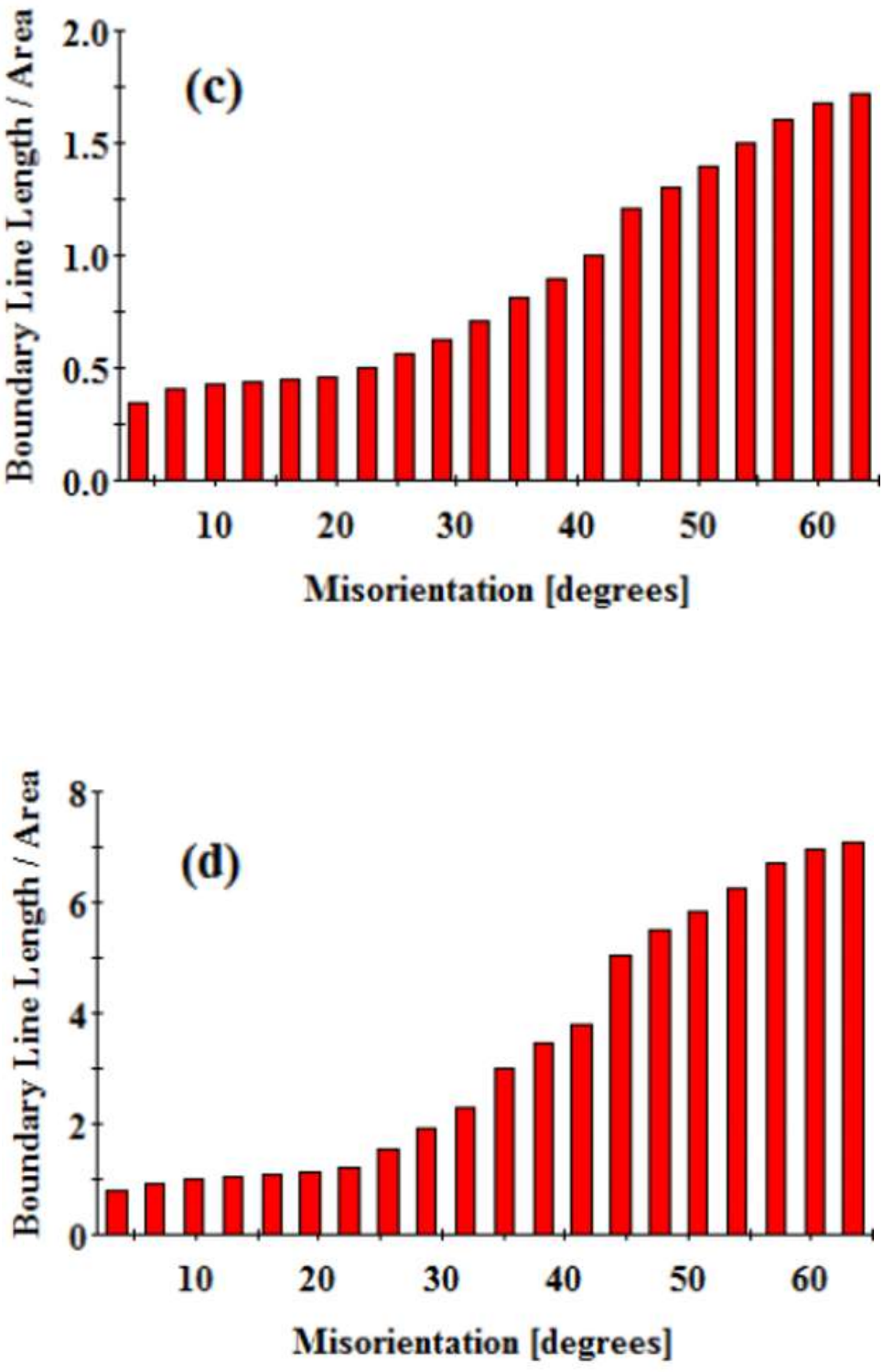

Figure 3.4: Grain boundary length/ unit area with misorientation angle distribution of low carbon steel of (c) ECAP-1.2, and (d) ECAP-1.8 samples.

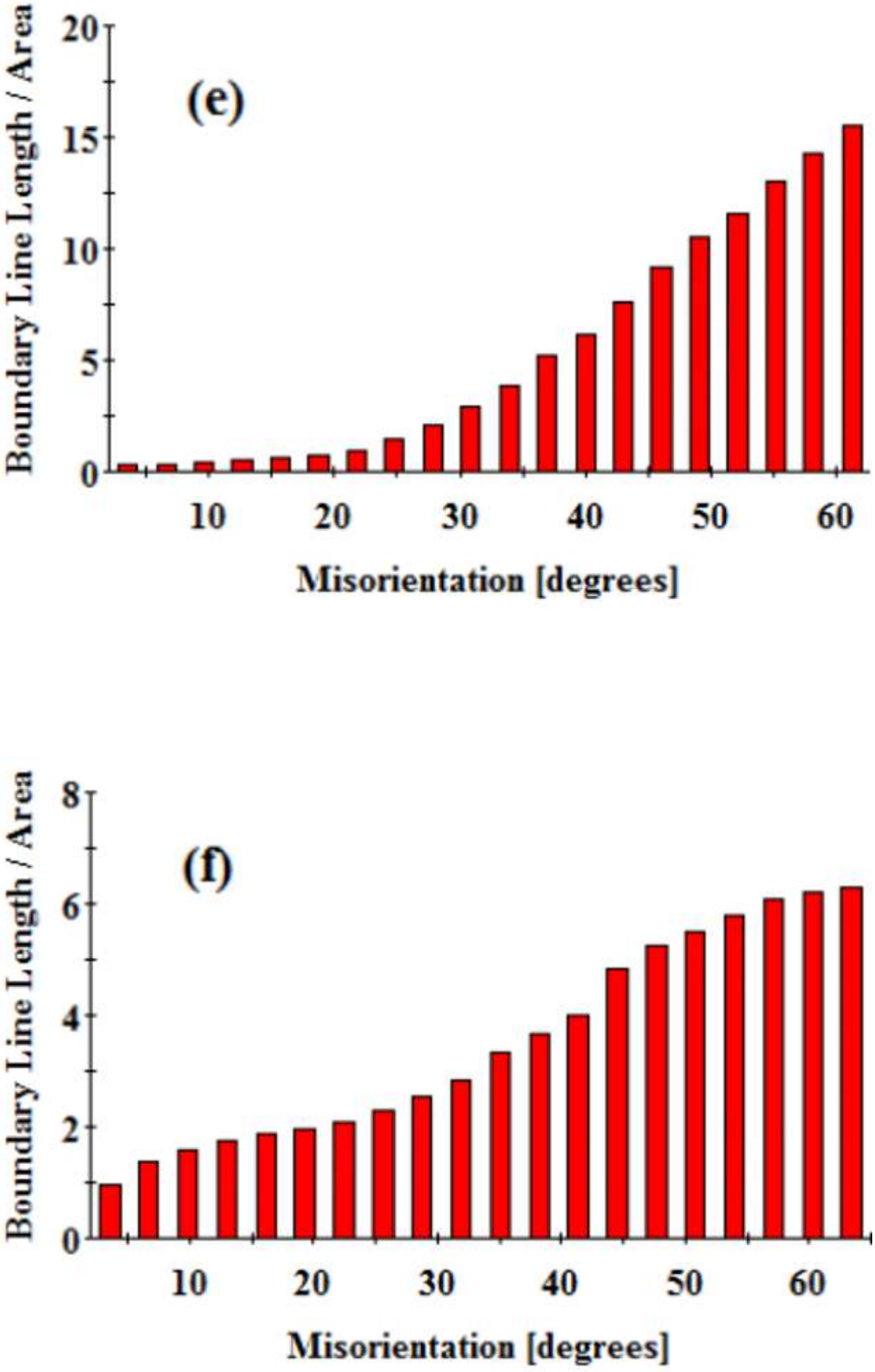

Figure 3.4: Grain boundary length/ unit area with misorientation angle distribution of low carbon steel of (e) ECAP-3, and (f) ECAP-6 samples.

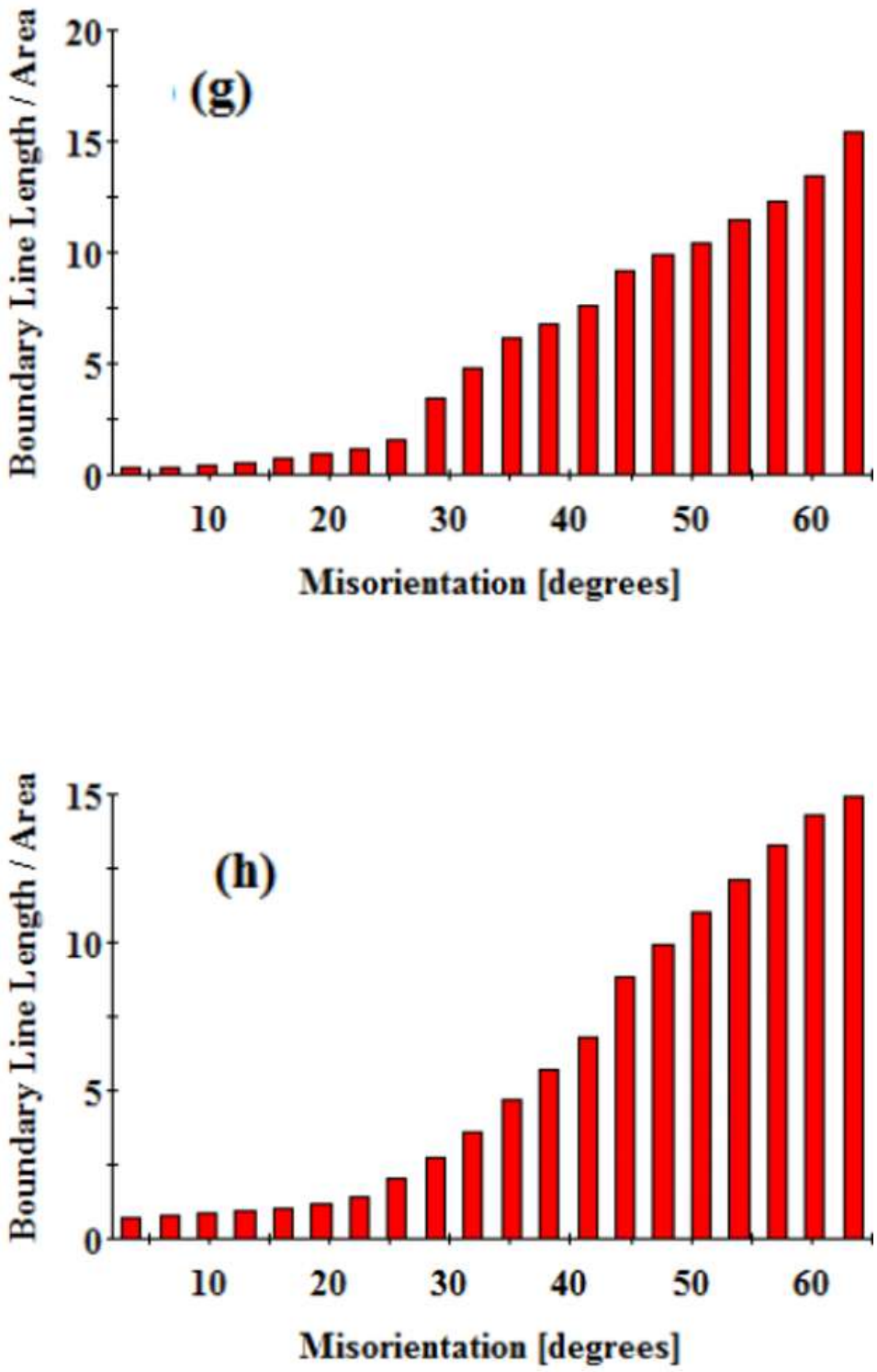

Figure 3.4: Grain boundary length/ unit area with misorientation angle distribution of low carbon steel of (g) ECAP-9, and (h) ECAP-12 samples.

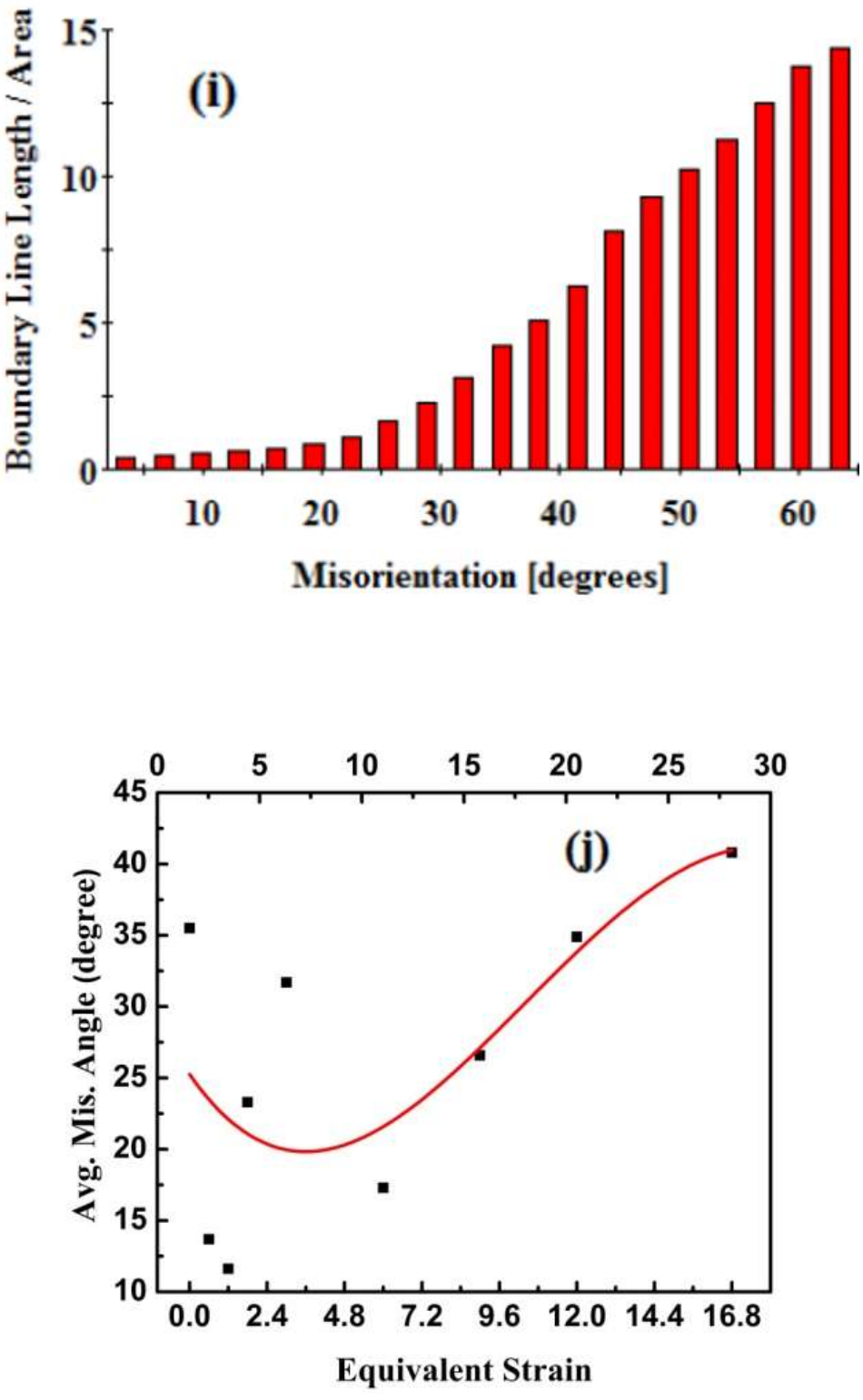

Figure 3.4: Grain boundary length/ unit area with misorientation angle distribution of low carbon steel of (i) ECAP-16.8 sample, and (j) Variation in average misorientation angle and equivalent strain of low carbon steel.

Figures 3.5-3.12 show TEM bright field images of ECAPed low carbon steel deformed upto a maximum strain of 16.8 along with their respective selected area diffraction (SAD) patterns. As-received low carbon steel contains low dislocation density of $1.8x10^{14}$ per m^2. At ε_{vm} = 0.6, grains get subdivided into bands of an average width of 620±110 nm (Figure 3.5(a)) with a low angle of misorientation (Figure 3.5(b)) and scattered high dislocation density of $10.3x10^{14}$ per m^2 (Table-3.1). At ε_{vm} = 1.2, the thickness of the deformation bands is decreased to 420±100 nm with a further low angle of misorientation (Figure 3.6(a), 3.6(b)), but the dislocation density further increased to 10.8 $x10^{14}$ per m^2(Table-3.1). At ε_{vm} = 1.8, the dislocation density not only reaches to a significantly high value of $28.4x10^{14}$ per m^2 but also the dislocations get scattered in the interior of the bands which have low angle of misorientation (Figure 3.7(a), 3.7(b)). At low strain range (ε_{vm} = 1.8) the cell blocks are aligned parallel to the deformation directions.

When the equivalent strain increases to 3, fragmentation of the bands takes place along with the alignment of bands towards deformation direction. The thickness of the bands decreases to 230±40 nm (Figure 3.8(a)), and the dislocation density decreases to $14.2x10^{14}$ per m^2 (Table 3.1). The fragmentation of bands takes place due to changes in the deformation direction between two successive passes into two orthogonal directions. At this strain level misorientation angle of the deformation bands and the cell block boundaries increase which is confirmed by sharp contrast of the boundaries of the bands and the corresponding diffraction pattern (Figure 3.8(b)).

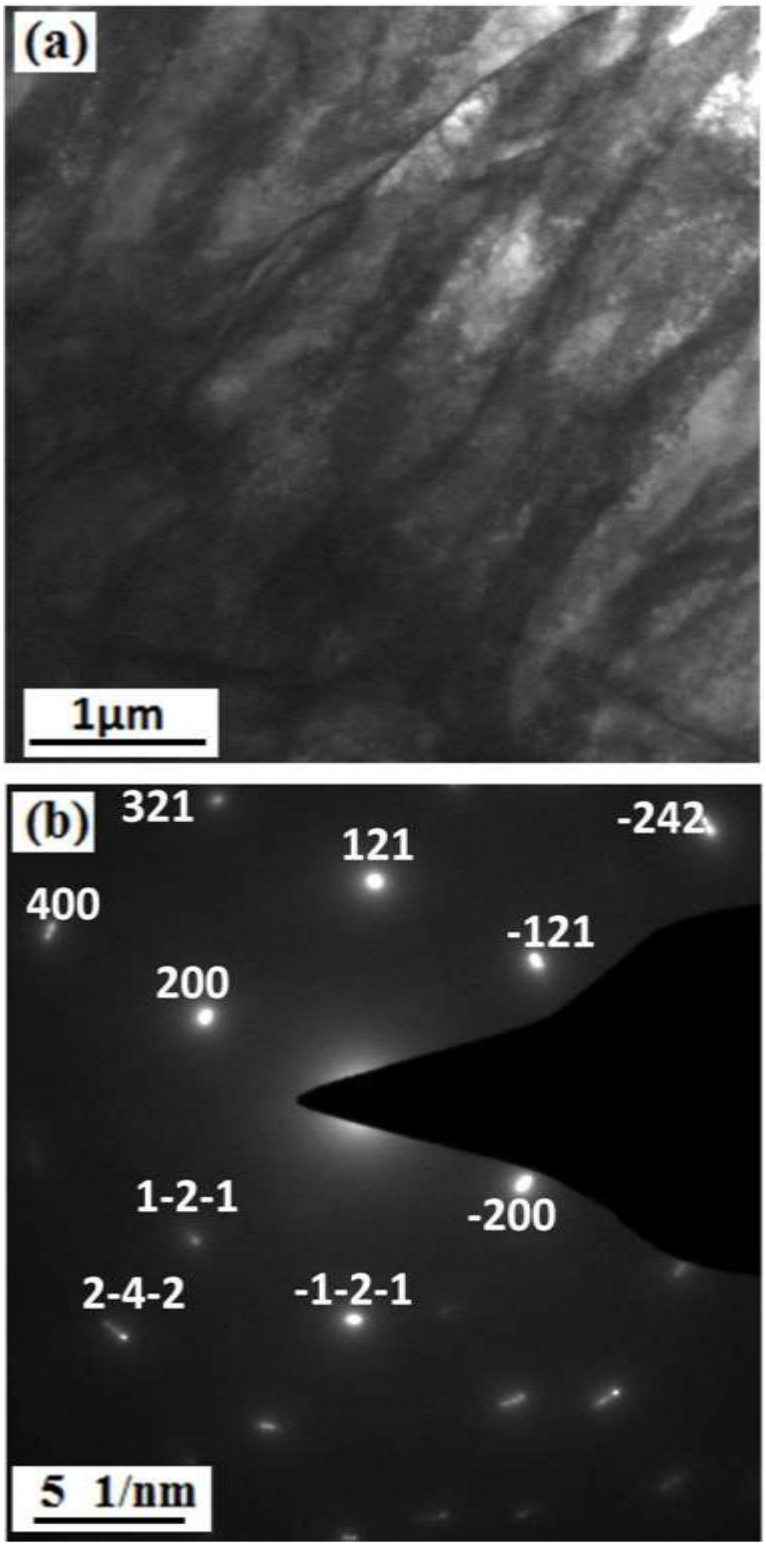

Figure 3.5: (a) TEM bright field image low carbon steel of ECAP-0.6, and (b) corresponding selected area diffraction pattern.

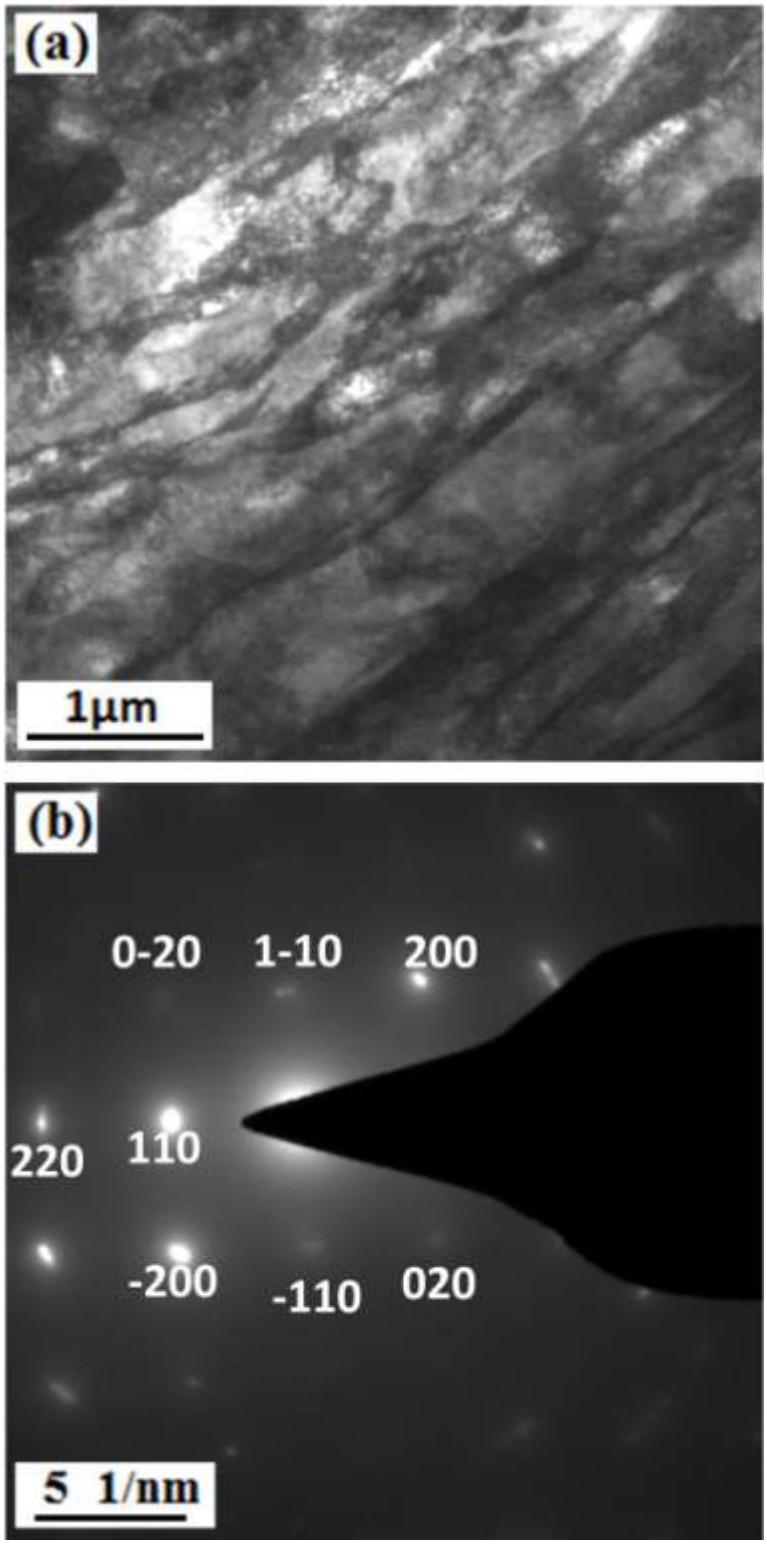

Figure 3.6: (a) TEM bright field image low carbon steel of ECAP-1.2, and (b) corresponding selected area diffraction pattern.

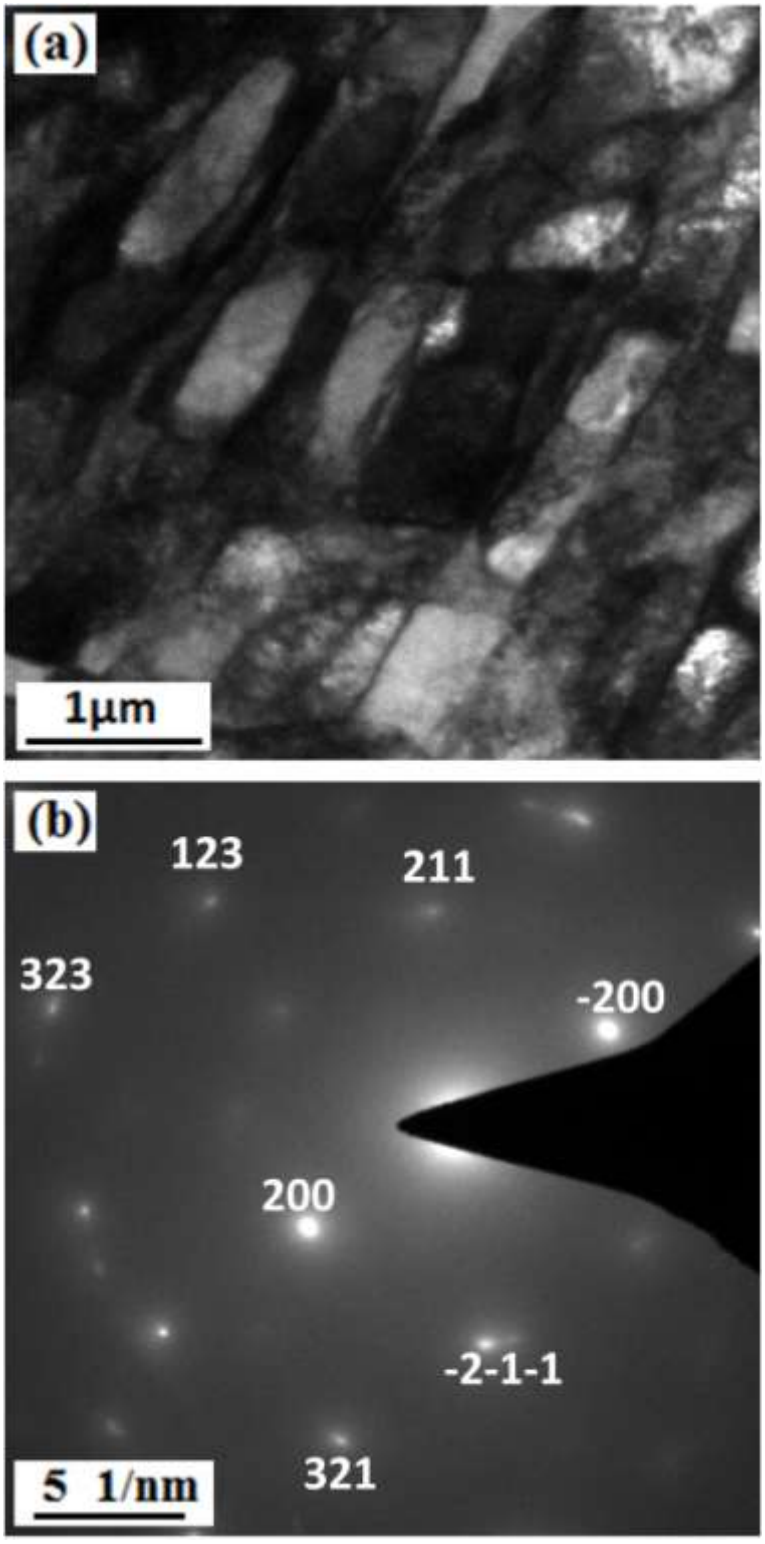

Figure 3.7: (a) TEM bright field image low carbon steel of ECAP-1.8, and (b) corresponding selected area diffraction pattern.

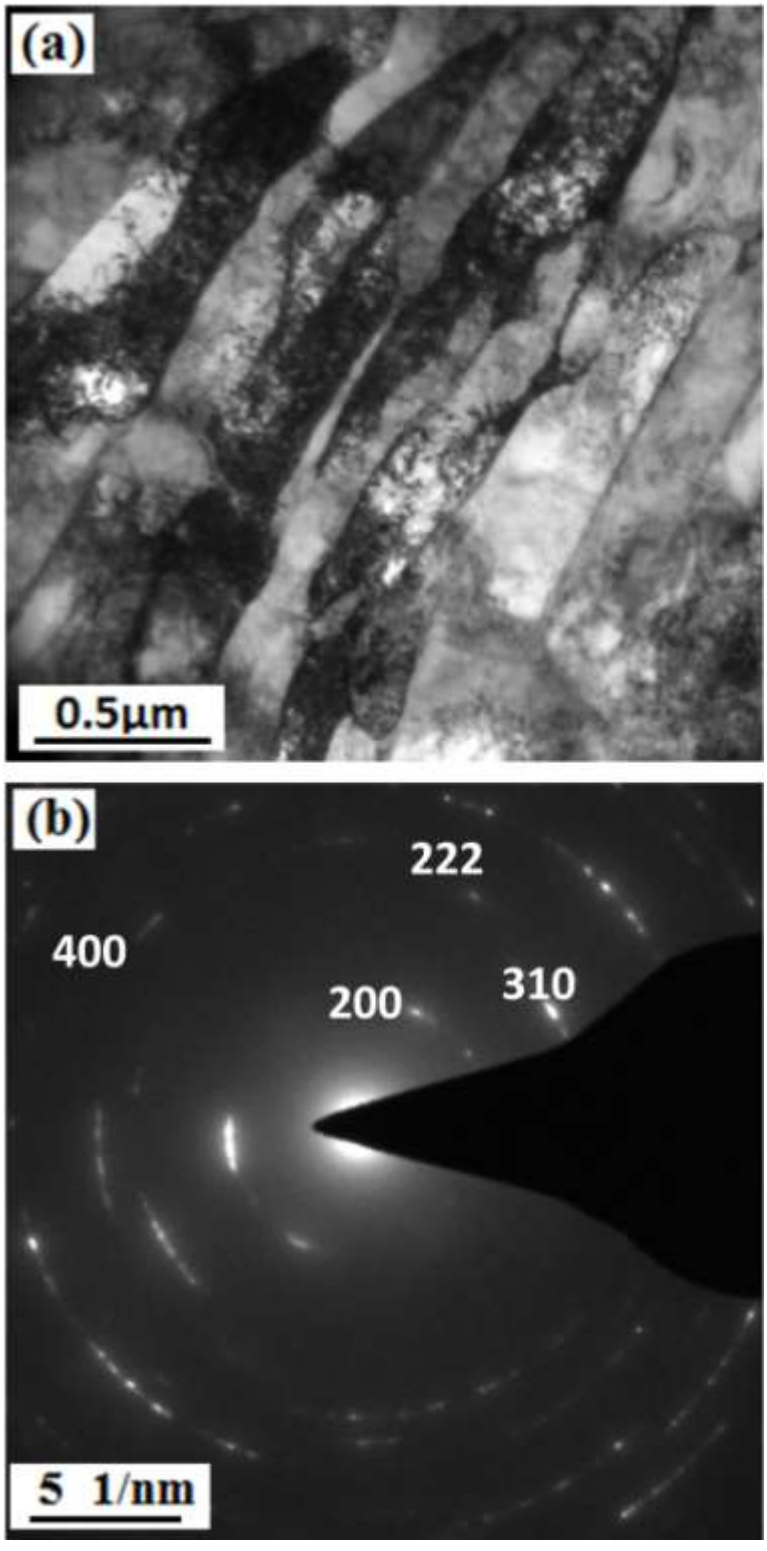

Figure 3.8: (a) TEM bright field image low carbon steel of ECAP-3, and (b) corresponding selected area diffraction pattern.

At ε_{vm} = 6, lamellar structures are produced by alignment of the high angle boundaries of the deformation bands and few cell block boundaries towards the deformation direction. Due to continuous straining misorientation angle of the deformation bands and the cell block boundaries further increase, and size decreases. Figure 3.9(a) shows some of the well-arranged cell block structures containing dislocation density of 15.1×10^{14} per m^2 along with the corresponding diffraction pattern confirming the large misorientation difference (Figure 3.9 (a), 3.9 (b)). The width of lamellar boundaries decreases to the width of a few subgrains, and their aspect ratio also increases with strain (at ε_{vm} = 9) (Figure 3.10 (a)). These lamellar boundaries are containing a large angle of misorientation (Figure 3.10 (b)). The thin bands which are one or two subgrains-wide are called ribbon grains. Even beyond ε_{vm} = 9 (at ε_{vm} = 12), the cell size further decreases but the rate of decrease in cell size with strain reduces, and the dislocation density becomes 14.7×10^{14} per m^2. The width of the ribbon grains decreases to single subgrain width (200 nm) (Figure 3.11(a)). These ribbon grains have a large angle of misorientation, confirmed by the corresponding diffraction pattern (Figure (3.11 (b)). At large strains ε_{vm} = 12-16.8, some of the ribbon grains split into the near-equiaxed grains. At ε_{vm} = 12-16.8 both ribbon as well as equiaxed grains coexist (Figures 3.11(a)-3.12(a)) with dislocation density, 17.1×10^{14} per m^2 (Table 3.1). The microstructure shows large angle, sharp equiaxed boundaries The grains are still in their metastable configuration even after ECAP at ε_{vm} = 16.8.

From x-ray line broadening analysis it is found that coherently scattering domain size in the as-received low carbon steel contains 137 nm (Table 3.1). On deformation at ε_{vm}=0.6 the domain size decreases to 40 nm. On further deformation domain size reaches a minimum value of 29 nm at ε_{vm}=16.8.

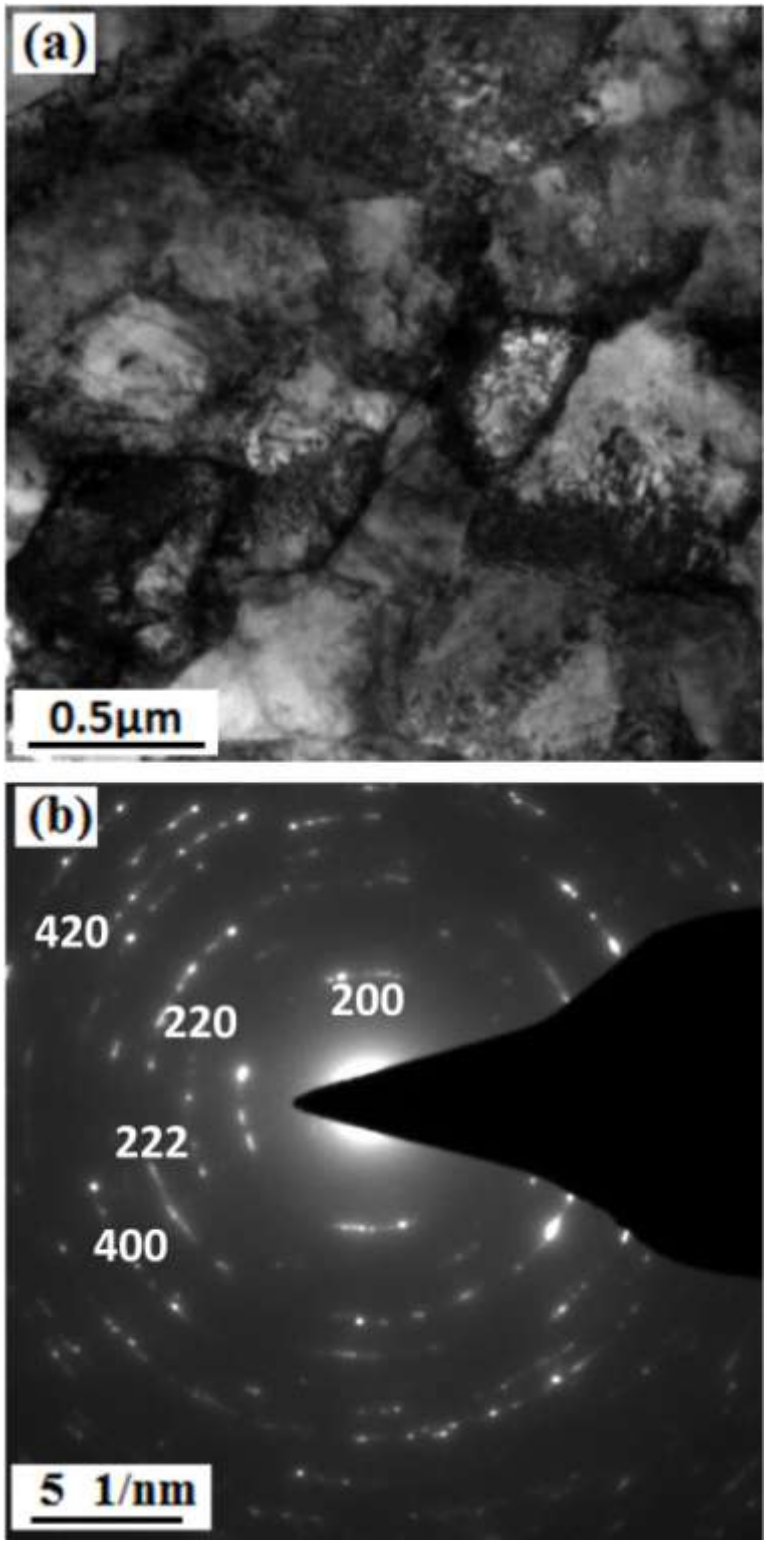

Figure 3.9: (a) TEM bright field image low carbon steel of ECAP-6, and (b) corresponding selected area diffraction pattern.

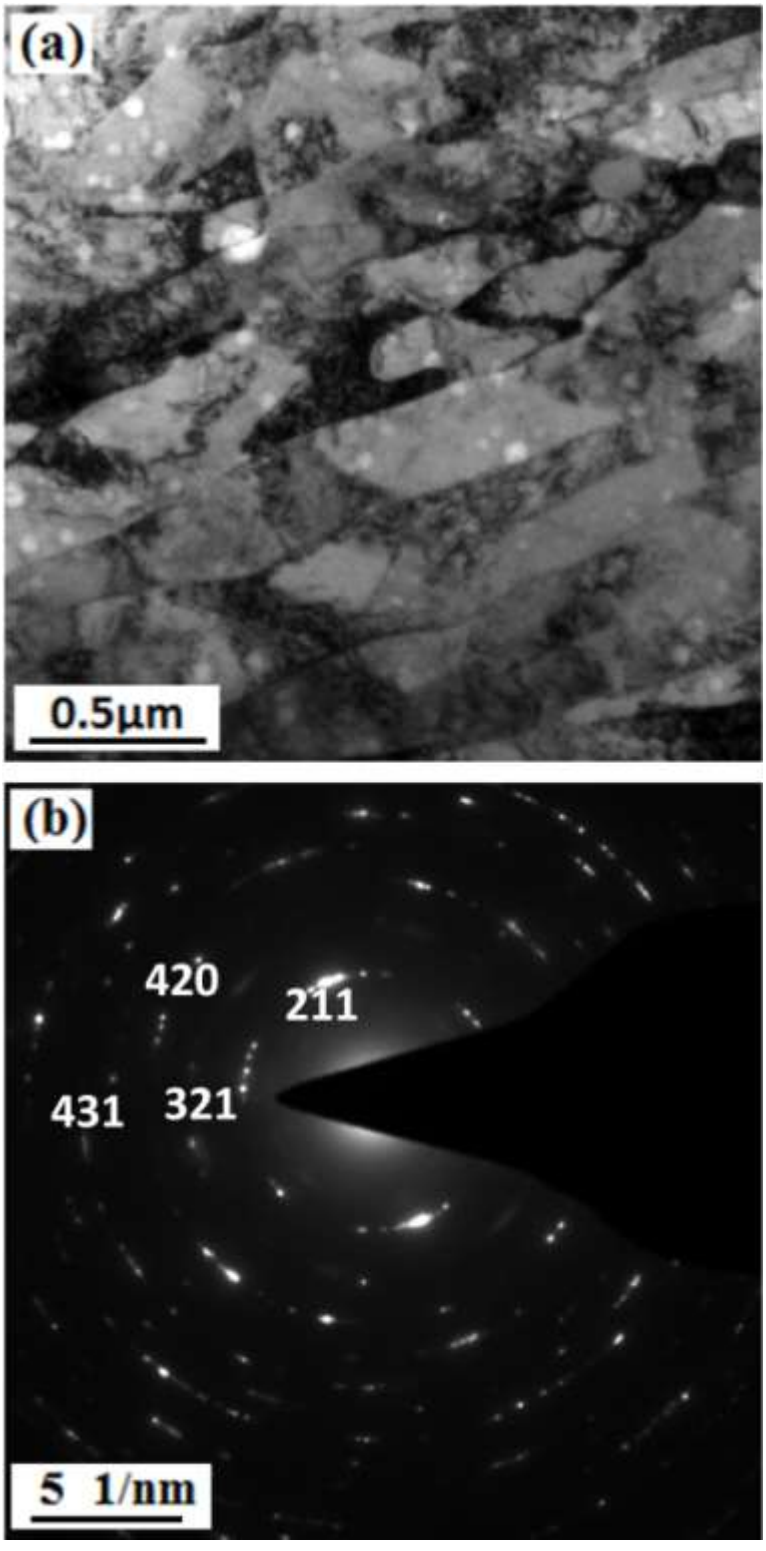

Figure 3.10: (a) TEM bright field image low carbon steel of ECAP-9, and (b) corresponding selected area diffraction pattern.

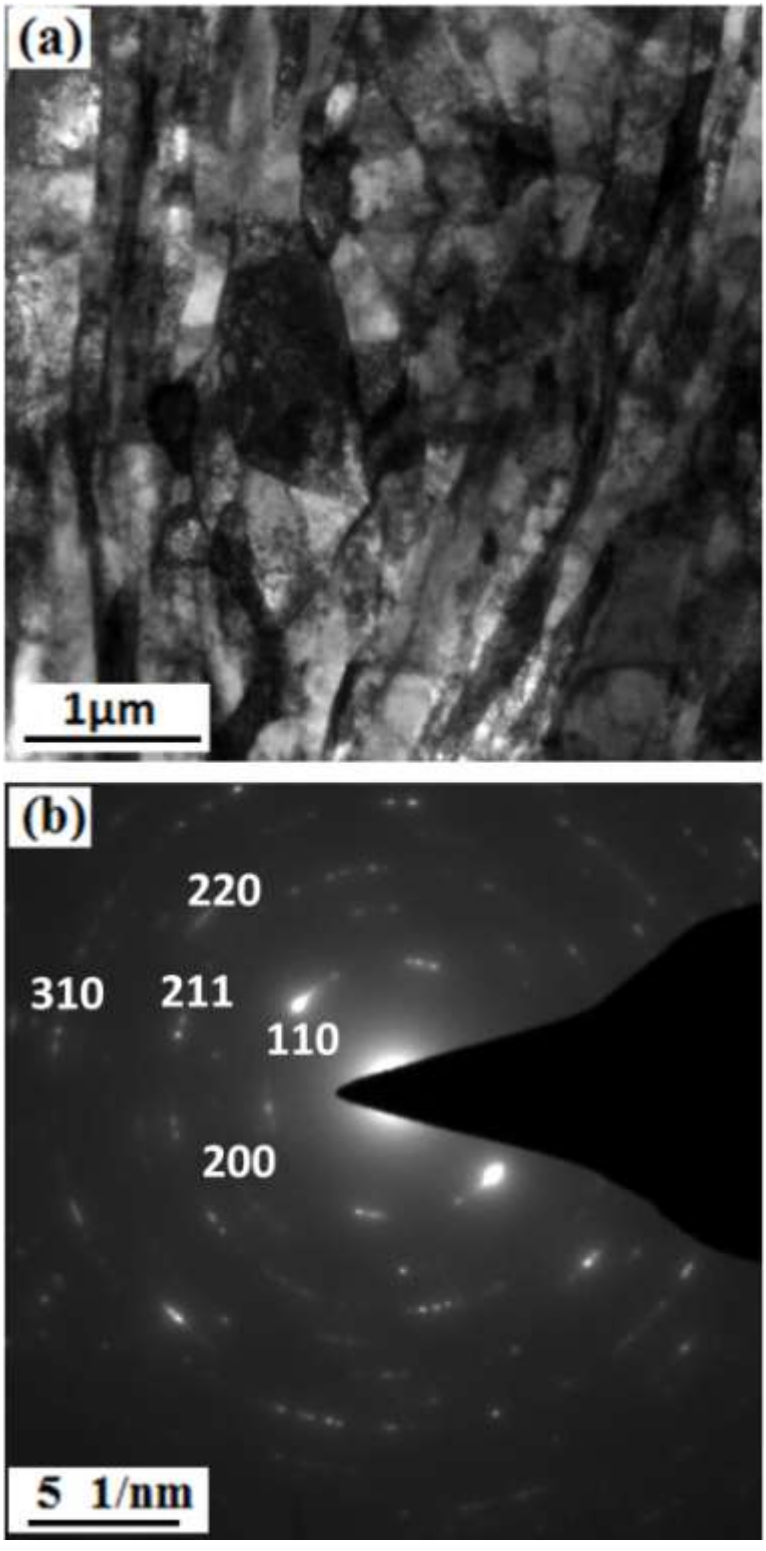

Figure 3.11: (a) TEM bright field image low carbon steel of ECAP-12, and (b) corresponding selected area diffraction pattern.

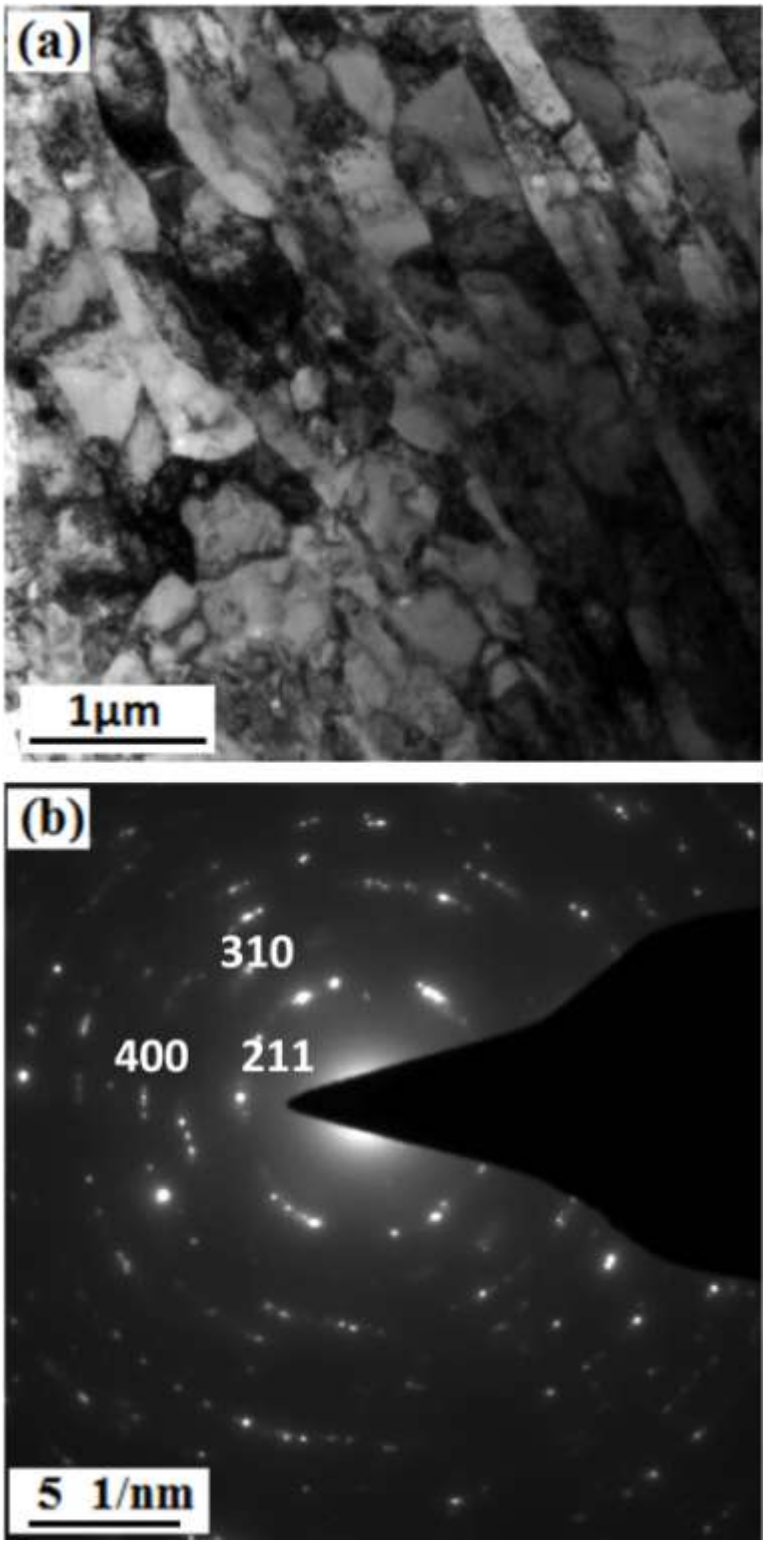

Figure 3.12: (a) TEM bright field image low carbon steel of ECAP-16.8, and (b) corresponding selected area diffraction pattern.

3.2 Discussion

The coarse-grained equiaxed microstructure of as-received low carbon steel gets modified to deformation bands with a high density of dislocations and reduced grain size at just $\varepsilon_{vm} = 0.6$. The deformation bands are formed due to the subdivision of the grains into regions of different orientations by the inhomogeneous stresses transmitted by neighboring grains [Humphreys et al. 1995]. The boundaries of deformation bands are thick and are of low angle of misorientation and contain a high density of dislocations. The dislocations are also scattered in the interior of bands. With the increase in strain to $\varepsilon_{vm} = 1.2$, the bands get elongated, and their thickness decreases. Rearrangement of dislocations causes dynamic recovery due to the increased interaction that leads to the decreased free path of dislocation which gives rise to LAGB formation. Some of the dislocations annihilate each other. During deformation, some part of the energy is stored in the material as dislocations, and the other part is dissipated as heat which causes dynamic recovery [Hodowany et al. 2000] with further reduction in domain size. At $\varepsilon_{vm} = 1.8$, the bands are separated by a cross-network of dislocations, and the cell structures develop at the interior of bands. A few cells form cell blocks. However, grain boundaries are partially revealed at $\varepsilon_{vm} = 1.8$ due to high micro-strain arising from high dislocation density. The increased value of elastic strain energy is related to increase in inhomogeneous strain distribution of dislocations inside the deformation bands.

As the imposed strain is increased to $\varepsilon_{vm} = 3$, an intersection of different bands in two orthogonal deformation directions give rise to fragmentation process. As a consequence of the rotation of large fraction of bands, most of the boundaries attain a high angle of misorientation. At $\varepsilon_{vm} = 6$, the boundaries of bands, few cell block boundaries, and grain boundaries all get aligned to the deformation direction resulting

in the lamellar structures. On straining, multiplication of dislocations increases elastic stored energy, although the grain size remains almost unchanged.

With the increase in strain, at ε_{vm} = 9, the lamellar width decreases to a few subgrain wide and their length increases. The elongated bands take the shape of ribbons. At ε_{vm} = 12, the width of each of the ribbon grains further decreases and becomes about one or two subgrains wide (Figure 3.11(a)) at few locations and their length increases to a high value. The misorientation angle increases and walls of ribbon grains become more sharp with increased interconnecting boundaries. A large value of stored energy is related to significant inhomogeneity in the microstructure. At ε_{vm} = 16.8, the ribbon grains are partially broken into near-equiaxed grain structure at many locations (shown by arrows (Figure 3.12(a))) with increased misorientation angle. These grains and subgrains are formed by the interaction of neighboring grains consequent to an increased rate of subgrain rotation [Prangnell et al. 2004]. Those ribbon grains which are slightly bent or curved are subdivided into grain or subgrain structure whereas straight ribbon grains are of high aspect ratio and their interconnecting boundaries are also straight and diffused, conforming the low angle of misorientation. At this strain level microstructure is heterogeneous (Figure 3.12(a)). Inhomogeneity in the plastic flow, formation of strong and weak texture components [Hutchinson et al. 1999], presence of large second phase particles [Humphreys et al. 1994] or shear banding accelerate fragmentation of ribbon grains. In general, the grain size is lower in low carbon steel in comparison to IF steel [Verma[b] et al. 2016] for a similar amount of imposed strain. Even though the initial microstructure for low carbon steel contains courser grains. Low angle boundary fraction is drastically lowered in low carbon steel for an equivalent amount of imposed strain. The average misorientation angle is also much higher in low carbon steel in comparison with IF

steel [Verma[b] et al. 2016]. Therefore the presence of carbon in steel enhances refinement process by severe plastic deformation. Low carbon steel contains high defect density. Incorporation of high amount of defects reduces grain size to a lower level and increases LAGBs, LAGBs get converted to HAGBs at a faster rate in low carbon steel. This results in high average misorientation angle. Severe plastic deformation increases the dislocation density at the low strain level. It reaches a maximum value at intermediate strain. With further increase in strain, dislocation density starts decreasing. Therefore, domain size reaches a minimum at the intermediate strain level beyond which it remains almost constant. Presence of carbon lowers the domain size for a similar equivalent strain. Therefore, domain size in low carbon steel is lower than that of interstitial-free steel [Verma et al. 2017].

At low strain level $\varepsilon_{vm} < 6$, mainly inter-lamellar spacing of pearlite reduces and dissolution of carbides begins at $\varepsilon_{vm} = 6$. At high strain level, cementite gets dissolved significantly and breaks down into isolated particles. Dissolution of cementite was reported earlier [Hono et al. 2001, Gavriljuk et al. 2003, Borchersa et al. 2009] at equivalent strain 1 in eutectoidal steel by wire drawing. It is also reported in the high carbon steel at a high strain of 53 imposed by high pressure torsion [Ivanisenko et al. 2002]. High pressure torsion of medium to high carbon steel (0.6-0.8wt%C) dissolves 40 % of cementite at $\varepsilon_{vm} = 36 – 58$, 60% dissolution and thinning of lamellae with fibrous structure at $\varepsilon_{vm} = 58 - 115$ but 100% dissolution takes place at $\varepsilon_{vm} = 115 - 174$ [Ivanisenko et al. 2003]. Cementite dissolution is triggered by the interaction of carbon with dislocations which cut the original crystalline cementite and then drag the carbon along, which is accommodated in the dilatational zone of the dislocation [Sauvage et al. 2007].

3.3 Summary

Equivalent strain of 16.8 can be imposed on low carbon steel by ECAP adopting route Bc at room temperature. On ECAP the grains get elongated at the initial stage of deformation, and the grains are subdivided into bands even at ε_{vm}=0.6. With increasing strain band thickness decreases at intermediate strain (ε_{vm}=1.8) and cellular structure is developed due to rearrangement of dislocations within the bands. Beyond a critical strain, dislocations are recovered, and their density decreases with imposed strain. At ε_{vm}=3, bands are partially fragmented, and at ε_{vm}=6, lamellar structure is formed. At ε_{vm}=9-12 bands get elongated, and ribbon grains are formed. At ε_{vm}=16.8, ribbon grains are partially broken down to near equiaxed structure due to an interaction of bands. In low carbon steel degree of refinement is higher than that of IF steel for similar amount of imposed equivalent strain due to the presence of carbon. The average misorientation angle reaches higher value and low angle grain boundary fraction also reduces to lower value at the high equivalent strain.

Therefore LAGB fraction increases at low strain level, reaches to a maximum at intermediate strain level and it continues to decrease with imposed strain and reaches a minimum at ε_{vm}=16.8. The degree of refinement is high at initial strain range ($\varepsilon_{vm} < 3$). It decreases with increasing strain. In low carbon steel pearlitic cementite starts dissolving at an equivalent strain low as 6. The dissolution increases with increasing strain, though it is not complete even at an equivalent strain of 16.8. Coarse-grained low carbon steel can be refined to 0.2 μm grain size by ECAP at an equivalent strain of 16.8.

Figure 3.4.1 (a) shows a variation in average boundary length/unit area with equivalent strain. Average boundary length per unit area is low for as-received low carbon steel. On imposing strain it increases rapidly up to an intermediate strain (1.8). Thereafter it increases at very slow rate in large strain range (Figure 3.4.1(a)).

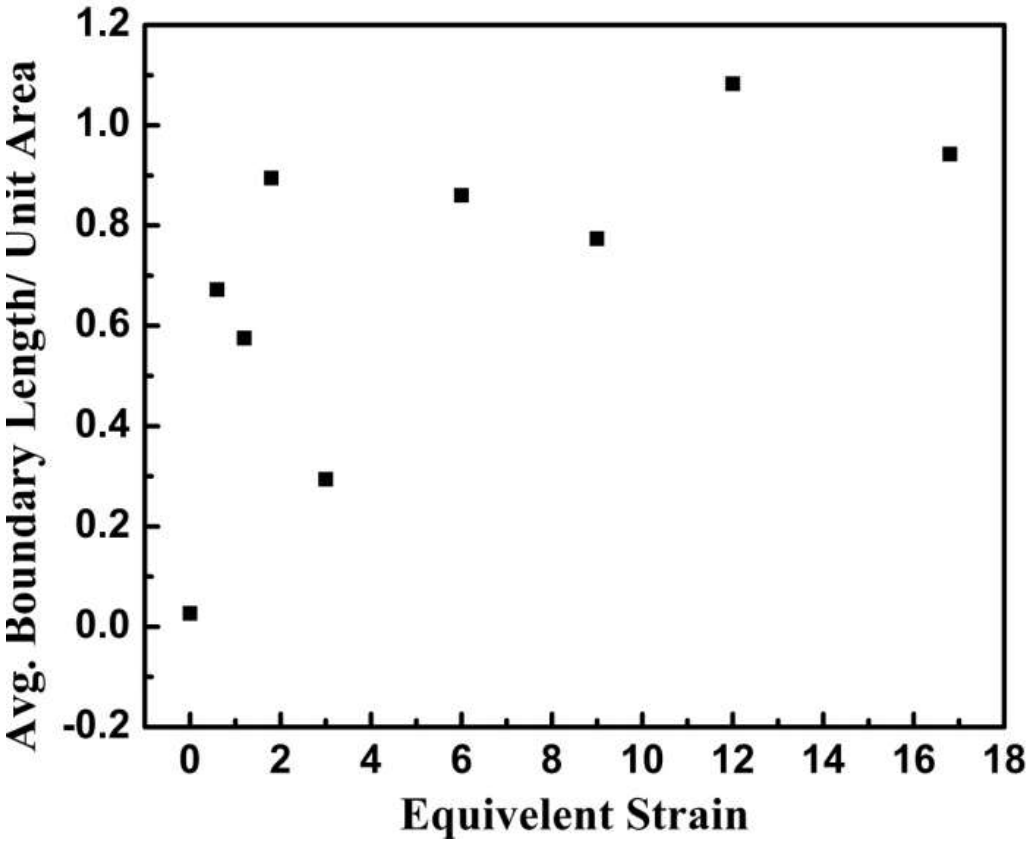

Figure 3.4.1 (a) Average boundary length/ unit area with equivalent strain (ε_{vm} = 0-16.8) for low carbon steel.

Boundary length/ unit area distribution in low to high angle of misorientation for equivalent strain 0-16.8 is shown in figure (Figure 3.4.1(b). Low angle boundary length is low for as-received low carbon steel. It increases with imposed strain at intermediate level (1.8) and it decreases at high strain range (Figure). Above two trends are closely matching with the LAGB vs. equivalent strain (Figure 3.4.1 (b)).

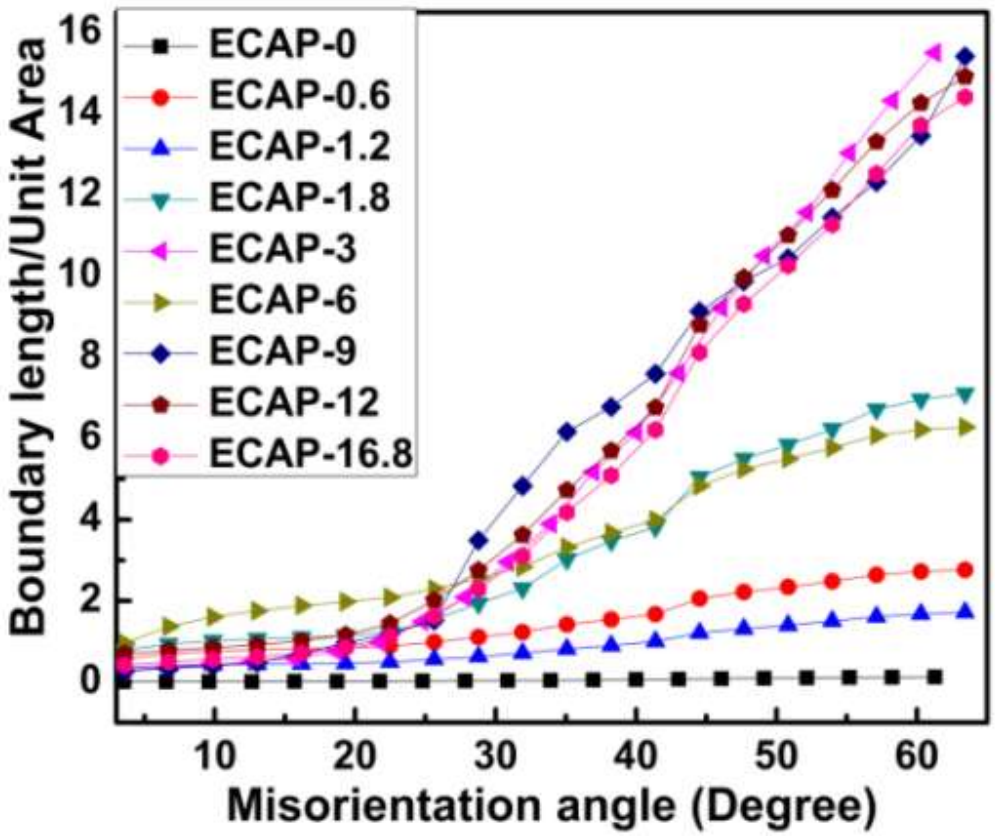

Figure 3.4.2 Boundary length per unit area distribution with misorientation angle for equivalent strain (ε_{vm} = 0-16.8).